Jefferson Lab PAC 39 Proposal
Timelike Compton Scattering and J/ψ photoproduction on the proton in e^+e^- pair production with CLAS12 at 11 GeV

I. Albayrak,[1] V. Burkert,[2] E. Chudakov,[2] N. Dashyan,[3] C. Desnault,[4] N. Gevorgyan,[3] Y. Ghandilyan,[3] B. Guegan,[4] M. Guidal*,[4] V. Guzey,[2,5] K. Hicks,[6] T. Horn*,[1] C. Hyde,[7] Y. Ilieva,[8] H. Jo,[4] P. Khetarpal,[9] F.J. Klein,[1] V. Kubarovsky,[2] A. Marti,[4] C. Munoz Camacho,[4] P. Nadel-Turonski*†,[2] S. Niccolai,[4] R. Paremuzyan*,[4,3] B. Pire,[10] F. Sabatié,[11] C. Salgado,[12] P. Schweitzer,[13] A. Simonyan,[3] D. Sokhan,[4] S. Stepanyan*,[2] L. Szymanowski,[14] H. Voskanyan,[3] J. Wagner,[14] C. Weiss,[2] N. Zachariou,[8] and the CLAS Collaboration.

[1] *Catholic University of America, Washington, D.C. 20064*
[2] *Thomas Jefferson National Accelerator Facility, Newport News, Virginia 23606*
[3] *Yerevan Physics Institute, 375036 Yerevan, Armenia*
[4] *Institut de Physique Nucleaire d'Orsay, IN2P3, BP 1, 91406 Orsay, France*
[5] *Hampton University, Hampton, Virginia 23668*
[6] *Ohio University, Athens, Ohio 45701*
[7] *Old Dominion University, Norfolk, Virginia 23529*
[8] *University of South Carolina, Columbia, South Carolina 29208*
[9] *Florida International University, Miami, Florida 33199*
[10] *CPhT, École Polytechnique, 91128 Palaiseau, France*
[11] *CEA, Centre de Saclay, Irfu/Service de Physique Nucléaire, 91191 Gif-sur-Yvette, France*
[12] *Norfolk State University, Norfolk, Virginia 23504*
[13] *University of Connecticut, Storrs, Connecticut 06269*
[14] *National Center for Nuclear Research (NCBJ), Warsaw, Poland*

(Dated: May 3, 2012)

We propose to measure exclusive e^+e^- production with CLAS12 and an 11 GeV polarized beam impinging on a hydrogen target to study the reaction $\gamma p \to \gamma^* p' \to e^+e^- p'$, known as Timelike Compton Scattering (TCS). Both the four-fold differential cross section and the cosine and sine moments of the weighted cross section will be measured over a wide range in $-t$, for outgoing photon virtualities Q'^2 up to 9 GeV^2. No prior TCS measurements exist except for pilot analyses of CLAS 6 GeV data, which demonstrated the general feasibility. The goals of the experiment are to gain fundamental insight into the nature of the Compton process in the partonic regime, to test the universality of GPDs by comparing spacelike and timelike DVCS (TCS), and to take advantage of the straightforward access in TCS to the real part of the Compton form factors, which will provide constraints on global GPD

*Co-spokesperson
†Contact person: turonski@jlab.org

fits. In addition, this experiment will provide a high-statistics measurement of the J/ψ photoproduction cross section near threshold.

Contents

1. INTRODUCTION

Understanding the structure and interactions of hadrons on the basis of Quantum Chromodynamics (QCD) is one of the main objectives of nuclear physics. The combination of fundamental properties of QCD as a quantum field theory, such as relativity and causality, with factorization theorems allows us to systematically explore the partonic structure of hadrons through various processes using different probes. In this context, the correspondence between spacelike and timelike processes plays a unique role, which can be illustrated by the following examples. First, we have the Drell-Yan process, $h\bar{h} \to \gamma^* X$, where γ^* has a timelike virtuality ($Q^2 > 0$) and h ($\bar{h}$) denotes a baryon (antibaryon), which provided important information on the (anti)quark distributions. A comparison of the Drell-Yan results with inclusive deep inelastic scattering (DIS), $\gamma^* h \to X$, mediated by a spacelike virtual photon ($Q^2 < 0$), demonstrated in a convincing way the universality of parton distribution functions (PDFs). Second, the detailed knowledge of the pion form factor, $F_\pi(t)$, in the timelike region ($t > 0$) can be used – with help of the dispersion relation – to determine $F_\pi(t)$ in a wide range of the spacelike region ($t < 0$), where the knowledge of $F_\pi(t)$ is poor, but essential for the determination of the transverse quark structure of the pion; for a recent analysis and references, see Ref. [1]. In this proposal we focus on the correspondence between spacelike and timelike deeply virtual Compton scattering (DVCS), where the latter is also known as timelike Compton scattering (TCS), and the universality of generalized parton distributions (GPDs).

In the last 15 years, hard exclusive processes have emerged as a class of reactions providing novel information on the quark and gluon distributions in hadrons. This information is more complete than what can be obtained from only inclusive and elastic scattering; for reviews, see Refs. [2, 3, 4]. QCD factorization theorems for exclusive processes [5, 6] allow one to express amplitudes of hard exclusive processes in terms of GPDs, which are expected to provide a universal (process-independent) description of the nucleon, and have a known QCD (Q^2) evolution. GPDs are hybrid distributions that combine aspects of the usual collinear PDFs and elastic form factors. As such, GPDs simultaneously encode information on parton distributions and correlations in both momentum (in the longitudinal direction) and coordinate (in the transverse direction) spaces. An interesting aspect of GPDs is also their connection to the form factors of the energy-momentum tensor, which, among other things, establishes the decomposition of the proton spin in terms of the quark and gluon contributions to the total orbital momentum [7].

The best studied hard exclusive process is DVCS, $\gamma^* p \to \gamma p$, where the initial-state virtual photon is spacelike ($Q^2 < 0$), and the final-state photon is real. From a theoretical point of view, it is the simplest and cleanest way to access GPDs. The leading-twist formalism is well established for DVCS at the leading and next-to-leading orders in the strong coupling constant, and power-suppressed corrections have been analyzed and estimated. On the experimental side,

early data have demonstrated the feasibility of DVCS measurements, established the reaction mechanism based on the leading-twist approach (the handbag mechanism), and provided first glimpses of the Compton form factors (CFFs) and GPDs. The goal of determining the valence quark GPDs in the nucleon through measurements of DVCS and other hard exclusive processes is now a cornerstone of the 12 GeV program at Jefferson Lab.

A new and promising opportunity on this road to measuring/constraining GPDs is presented by the process of timelike Compton scattering (TCS), $\gamma p \to \gamma^* p$, where the final-state photon has a timelike virtuality ($Q'^2 > 0$). The leading-twist formalism for TCS [8] (the factorization theorem, the handbag reaction mechanism, etc) is as well established as that for DVCS. However, as also shown in Ref. [8], the phenomenology of TCS is quite different from DVCS. With an unpolarized photon beam, TCS offers straightforward access to the real part of the CFFs through the interference between the Compton and Bethe-Heitler (BH) amplitudes, which can be extracted in a model-independent way from the azimuthal angular distribution of the lepton pair into which the timelike photon decays. Circular photon polarization also gives access to the imaginary part of CFFs. The main motivations to study TCS thus include:

- A measurement of TCS will make it possible to test the universality of GPDs implied by factorization through the timelike-spacelike correspondence with DVCS.

- The straightforward access in TCS to, in particular, the real part of the CFFs through cosine moments of the weighted cross section impacts models and parametrizations of GPDs in a broad range of kinematics (light-cone fractions x and η, where η is the equivalent of ξ in DVCS).

- The differential cross section (including TCS and its interference with BH) can provide important input for global fits of CFFs [9].

The feasibility of TCS measurements has recently been demonstrated by pilot analyses of CLAS 6 GeV data, but a dedicated 12 GeV experiment is required in order to reach the resonance-free region in the lepton invariant mass between the ρ' and the J/ψ, to extend the kinematic coverage, and to collect sufficient statistics. The interest in TCS is also growing in view of the possibility to experimentally study it in ultraperipheral collisions, for instance at the LHC [10].

In addition to studying TCS, we also plan to make a high-statistics measurement of the J/ψ photoproduction cross section on the proton. This measurement is very interesting in its own right, and will be an early result from CLAS12. It will shed light on the reaction mechanism near threshold, and provide unique insights into the gluonic structure of the nucleon at large x. Within the GPD framework, this reaction would probe kinematics with large skewness (ξ) close to threshold. One could, however, also interpret it as a measurement of the gluonic form factor

of the nucleon at a relatively high value of $|t|$. In addition, the measurement of the J/ψ cross section will be valuable for understanding the systematics within the TCS data, in particular if we can run with both polarities of the torus field.

Encouraged by the positive recommendation from PAC38 for our letter of intent (LOI11-106), "The physics addressed in this proposal is very relevant for the JLab 12 GeV program. The PAC encourages the development of a full proposal.", we thus propose to measure exclusive e^+e^- production with CLAS12 and an 11 GeV linearly polarized electron beam impinging on a hydrogen target to study TCS and J/ψ production with quasi-real photons in the reaction $ep \to e^+e^-p(e')$. We will measure both the four-fold differential cross section and, for TCS, also the cosine and sine moments of the weighted cross section.

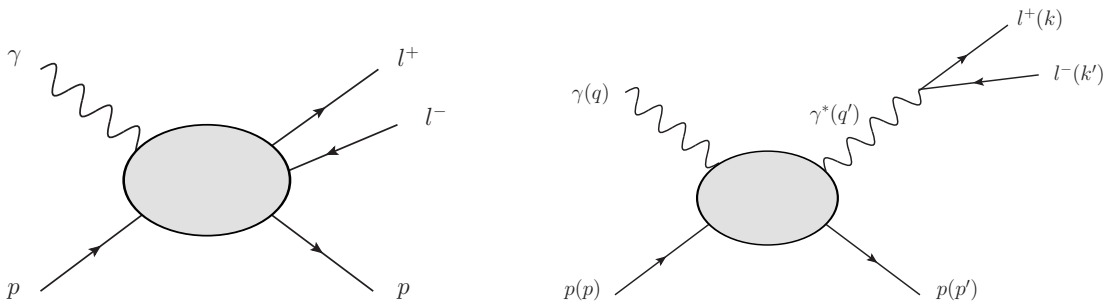

FIG. 1: *Left panel:* Exclusive photoproduction of a lepton pair. *Right panel:* Timelike Compton scattering (TCS). The particle momenta are given in parenthesis.

2. PHYSICS OF TIMELIKE COMPTON SCATTERING

In this section we describe the theory and phenomenology of the timelike Compton process, discuss observables, and present model calculations. We also explain how the data can be used in global fits, and show 6 GeV analysis results.

A. Kinematics

Timelike Compton Scattering (TCS),

$$\gamma(q) + p(p) \to \gamma^*(q') + p(p')\,, \tag{1}$$

is the process of photoproduction of a virtual timelike photon ($q'^2 = Q'^2 > 0$) on a nucleon. As shown in the right panel of Fig. 1, the final-state virtual photon immediately decays into a lepton pair. TCS is, however, not the only physical processes that can be observed in exclusive photoproduction of lepton pairs, $\gamma p \to l^+ l^- p$. Another process with the same final state is the purely electromagnetic Bethe-Heitler (BH) reaction shown in Fig. 2. Like in DVCS, the TCS and BH amplitudes interfere. In JLab 12 GeV kinematics, where the BH cross section is significantly larger than the TCS cross section, one can take advantage of this interference to enhance the TCS signal; see Sect. 2 C for details.

The TCS amplitude depends on the following three kinematic invariants:

$$\begin{aligned} q'^2 &= Q'^2 > 0\,, \\ s &= (p+q)^2\,, \\ t &= (p'-p)^2\,, \end{aligned} \tag{2}$$

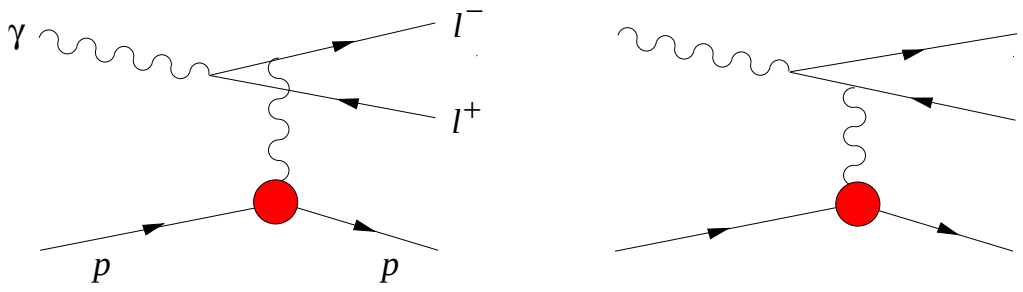

FIG. 2: The Feynman graphs for the Bethe-Heitler contribution to the $\gamma p \to l^+ l^- p$ process.

where $q'^2 = Q'^2$ is the virtuality of the final-state photon, s is the invariant photon-proton energy squared, and t is the four-momentum transfer squared. In addition to these three variables, the $\gamma p \to l^+ l^- p$ cross section depends on the angles θ and φ associated with the final-state lepton pair. In the $l^+ l^-$ center-of-mass frame, θ is the angle between the momenta of the lepton $\vec{k}$ and the recoiling proton $\vec{q'}$, and φ is the angle between the reaction plane and the lepton decay plane, as shown in Fig. 3.

B. Leading-twist formalism

To ensure the applicability of the leading twist formalism to the $\gamma p \to l^+ l^- p$ process (left panel of Fig. 2, one requires that (i) the timelike virtuality of the final-state photon, Q'^2, is sufficiently large to provide a hard scale, (ii) the invariant photon-proton c.m. energy, $\sqrt{s}$, is sufficiently large to ensure the usual DIS kinematics, and (iii) the invariant momentum transfer squared t is low, *i.e.*, $|t| \leq 1$ GeV^2. The timelike nature of the final state also makes interpretation complicated in the presence of resonances in the invariant mass of the produced lepton pair. Hence, as shown in Fig. 4, an ideal mass range for this experiment is $M_{\rho'} < M_{l^+l^-} < M_{J/\psi}$, which coincides well with JLab 12 GeV kinematics. Since the invariant mass of the lepton pair, $M_{l^+l^-}$, is also the timelike virtuality of the outgoing photon, Q', focusing on the resonance-free region automatically satisfies condition (i) above.

The leading-twist formalism for TCS has been developed in Ref. [8]. It is based on the factorization theorem [6] that allows one to express the TCS amplitude in Eq. (1) as convolutions of calculable hard-scattering kernels with GPDs. The resulting quantities are called Compton form factors (CFFs). One expects that as long as Q'^2 is sufficiently large, the leading-twist approximation (*i.e.*, ignoring terms of the order of m_N^2/Q'^2, m_l^2/Q'^2, and $|t|/Q'^2$) should work equally well for TCS as it does for DVCS. In other words, one does not expect enhanced higher twist corrections specific to TCS [3].

To leading order in the strong coupling constant, α_s, the TCS amplitude is given by

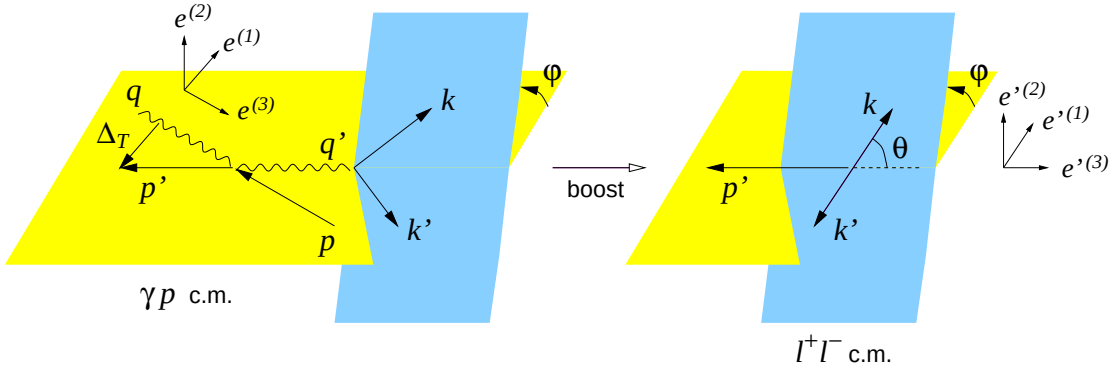

FIG. 3: Momenta and angles involved in the TCS cross section in the γp and l^+l^- center-of-mass frames. Adopted from [8]. Note that the angles φ and θ will be referred to explicitly as φ_{CM} and θ_{CM} outside of the motivation section to avoid confusion with the angles in the lab system.

the two handbag diagrams presented in Fig. 5. To leading order in α_s, the TCS amplitude is equivalent to the DVCS amplitude, making it easier to test the universality of GPDs. However, at the next-to-leading order, the expressions for the hard scattering kernels for TCS and DVCS are different and, as a result, the TCS and DVCS CFFs have different forms [11, 12]. This is discussed further in Sect. 2 D.

The proton has four leading-twist parton-helicity non-flip GPDs. The expressions for the corresponding CFFs, $\mathcal{H}_1$, $\mathcal{E}_1$, $\tilde{\mathcal{H}}_1$, and $\tilde{\mathcal{E}}_1$ are:

$$\begin{aligned}
\mathcal{H}_1(\eta,t) &= \sum_q e_q^2 \int_{-1}^{1} \left(\frac{H^q(x,\eta,t)}{\eta - x + i\epsilon} - \frac{H^q(x,\eta,t)}{\eta + x + i\epsilon} \right) , \\
\mathcal{E}_1(\eta,t) &= \sum_q e_q^2 \int_{-1}^{1} \left(\frac{E^q(x,\eta,t)}{\eta - x + i\epsilon} - \frac{H^q(x,\eta,t)}{\eta + x + i\epsilon} \right) , \\
\tilde{\mathcal{H}}_1(\eta,t) &= \sum_q e_q^2 \int_{-1}^{1} \left(\frac{\tilde{H}^q(x,\eta,t)}{\eta - x + i\epsilon} + \frac{\tilde{H}^q(x,\eta,t)}{\eta + x + i\epsilon} \right) , \\
\tilde{\mathcal{E}}_1(\eta,t) &= \sum_q e_q^2 \int_{-1}^{1} \left(\frac{\tilde{E}^q(x,\eta,t)}{\eta - x + i\epsilon} + \frac{\tilde{E}^q(x,\eta,t)}{\eta + x + i\epsilon} \right) ,
\end{aligned} \tag{3}$$

where the superscript q denotes the quark flavor and e_q the quark charge. For brevity, we suppressed the Q^2-dependence of the GPDs and CFFs. In Eq. (3), the light-cone fraction η, which in TCS plays the role of the skewness ξ in DVCS, is fixed by the external kinematics:

$$\eta = -\frac{(q-q')\cdot(q+q')}{(p+p')\cdot(q+q')} \approx \frac{Q'^2}{2s - Q'^2} \,. \tag{4}$$

From Eq. (3) it follows that the imaginary part of the CFFs can be expressed in terms of GPDs along the so-called cross-over line, *i.e.*, at $x = \eta$ for quarks and $x = -\eta$ for antiquarks.

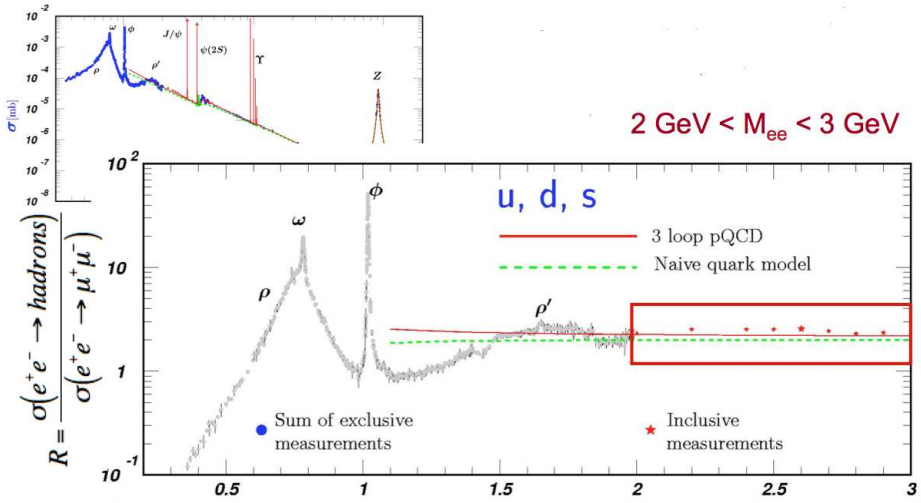

FIG. 4: Measurements of e^+e^- annihilation into hadrons show a resonance-free window between the ρ' and the J/ψ, which is ideal for TCS studies with CLAS after the 12 GeV upgrade.

The real part of the CFFs is, on the other hand, sensitive to GPDs over the entire range of x. For instance, the real part of the CFF $\mathcal{H}_1$ is given by:

$$\Re e\mathcal{H}_1(\eta,t) = \sum_q e_q^2\, p.v. \int_{-1}^{1} \left(\frac{H^q(x,\eta,t)}{\eta - x} - \frac{H^q(x,\eta,t)}{\eta + x} \right) , \tag{5}$$

where $p.v.$ stands for the principal value. The straightforward access to the real part of CFFs (see Sect. 2 C) gives TCS measurements the potential to constrain GPDs away from the cross-over line in a wide range of x and η.

The imaginary part of the Compton amplitude is now relatively well understood, primarily through measurements of DVCS. However, much less is known about the real part, which may become important at larger values of x, coinciding with JLab 12 GeV kinematics. The limited knowledge of the real part of the amplitude is reflected in GPD model predictions, which are in good general agreement for the imaginary part, but differ significantly when it comes to the real one. This is illustrated in Figs. 6 and 7, which show the real and imaginary parts of the GPD H as a function of x and $-t$, respectively, for two GPD models: the dual parametrization [13, 14, 15, 16] and the double distribution [17]. The potential of TCS to provide additional constraints on the real part of CFFs is thus important for developing more accurate GPD models. The TCS data could also be used in global fits of CFFs and for dispersion relation analysis. This is discussed in more detail in Sect. 2 E and Sect. 2 F, respectively.

In TCS, the use of a circularly polarized photons allows a determination of both the real and imaginary parts of the helicity amplitudes or CFFs with comparable uncertainties. In contrast, DVCS measurements strongly favor the imaginary part. The real part is only

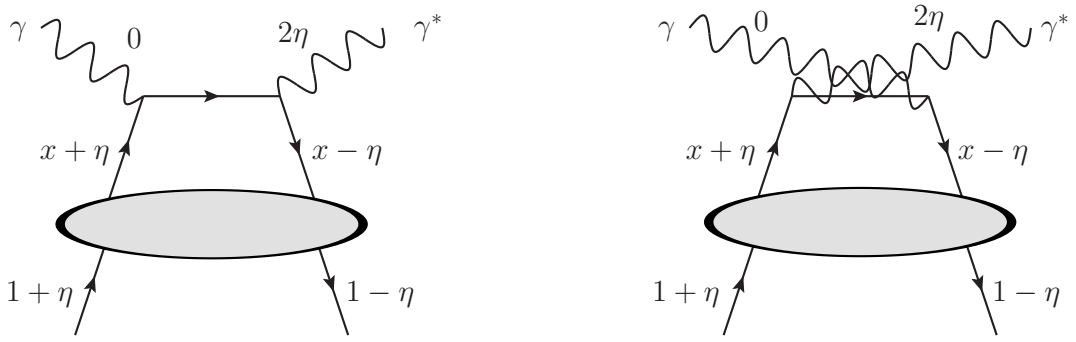

FIG. 5: The handbag diagrams for TCS. The plus-momentum fractions refer to the average proton momentum $(p+p')/2$.

available through direct cross section measurements or comparisons of cross sections measured with electron and positron beams, both of which are significantly more challenging than, for instance, the measurement of beam spin asymmetries that give access to the imaginary part.

In addition to discriminating between GPD models and constraining fits of CFFs, a measurement of TCS may also offer a unique possibility to address the issue of the so-called D-term [18]. Technically, the D-term is defined as the contribution to the GPD H that provides the highest power of ξ in Mellin moments of this GPD. The D-term of the GPD E has the same magnitude but opposite sign. The D-term contribution to GPDs has support only in the region $x \in [-\eta, \eta]$, which makes it elusive and inaccessible in the forward limit. This unambiguously indicates that the D-term cannot be interpreted in terms of the usual parton densities. Instead, the D-term describes the emission of a $q\bar{q}$ pair by the nucleon, revealing the complex nature of the nucleon as a many-body system.

The distribution of energy, momentum, and angular momentum in the nucleon is characterized by form factors of the QCD energy-momentum tensor between the nucleon states [7, 19], all of which can be expressed in terms of GPDs. The D-term gives rise to one of these form factors (denoted $C(t)$ or $d_1(t)$ in the literature).

It has been shown that in the Breit frame, this form factor can be interpreted as describing the distribution of pressure and shear forces acting on quarks inside the nucleon [20]. Studies in field-theoretical models show that the negative sign of the D-term is a consequence of the stability of the nucleon [21]. This is illustrated in Fig. 8, where the pressure $p(r)$ experienced by quarks inside the nucleon is given as a function of the distance from the center, r. Stability arises as a balance between repulsive forces in the inner region, and attractive forces at large r, such that the stability condition $\int_0^\infty \mathrm{d}r\, r^2 p(r) = 0$ holds. The D-term is given by $d_1 = 5\pi M \int_0^\infty \mathrm{d}r\, r^4 p(r)$ and the additional weight r^2 in the integrand emphasizes the role of large distances and binding

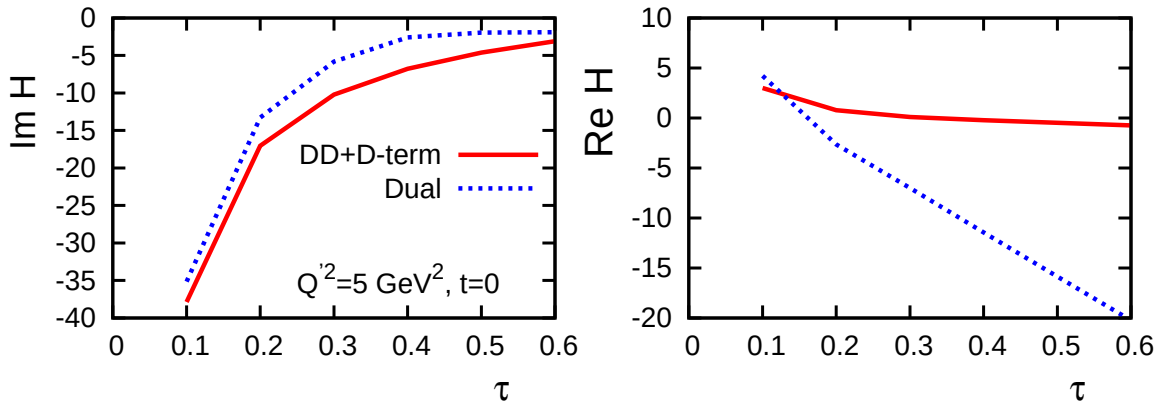

FIG. 6: Imaginary (left) and real (right) parts of the GPD H plotted as a function of $\tau = Q'^2/(s-M^2)$, which is the TCS equivalent of Bjorken x, for $Q'^2 = 5$ GeV^2 and $t = 0$. The curves correspond to GPD models based on the dual parametrization [13, 14, 15, 16] and the double distribution [17], respectively.

forces inside the nucleon, leading to a negative value of the D-term [21].

Form factors of the QCD energy-momentum tensor can also be calculated from first principles in lattice QCD. The QCDSF collaboration calculated the D-term form factor $d_1(t)$ as a function of $-t$ for the pion mass $m_\pi = 640$ MeV [22]. The predictions of the chiral quark-soliton model [21] used for the calculation shown in Fig. 8 are in agreement with the lattice data.

The notion of the D-term is also important for phenomenology because it (i) gives an energy-independent (η-independent) contribution to $\Re e H_1$ and $\Re e E_1$, and (ii) determines the subtraction constant in the dispersion relation connecting the real and imaginary parts of the TCS and DVCS amplitudes [23, 24, 25]. In the language of Regge theory [26, 27, 28, 29], the D-term can be interpreted as originating from the t-channel exchange with $J = 0$ (the so-called fixed pole).

C. TCS cross section and interference between TCS and BH amplitudes

In the leading-twist approximation, the TCS cross section has the following form [8]:

$$\frac{d\sigma_{\rm TCS}}{dQ'^2\, dt\, dcos\theta\, d\varphi} \approx \frac{\alpha_{\rm em}^3}{8\pi s^2}\frac{1}{Q'^2}\frac{1+\cos^2\theta}{4}\sum_{\lambda,\lambda'}|M^{\lambda',-\lambda}|^2\,, \tag{6}$$

where $\alpha_{\rm em}$ is the fine structure constant and $M^{\lambda',-\lambda}$ are helicity amplitudes, with λ (λ') denoting the helicity of the incoming (outgoing) photon. The TCS amplitude squared entering

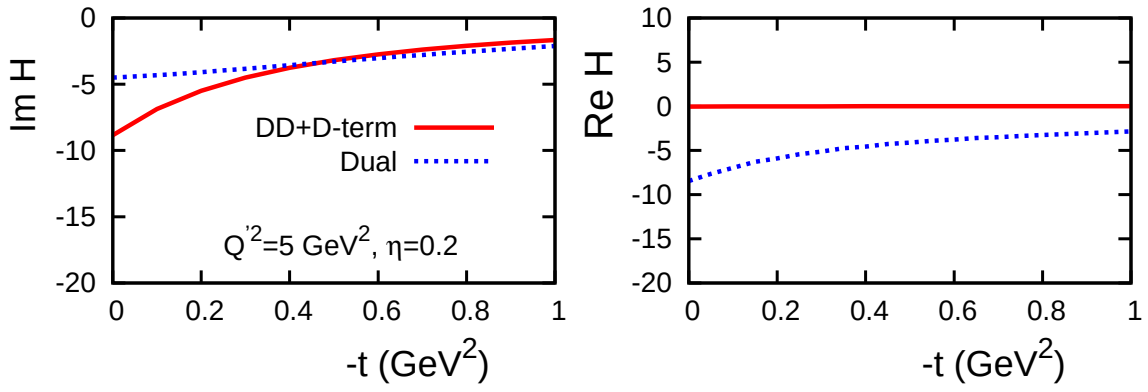

FIG. 7: Imaginary (left) and real (right) parts of the GPD H plotted as a function of $-t$ for $Q'^2 = 5$ GeV^2 and $\eta = 0.2$ (*i.e.*, $\tau = 0.33$), where η is the TCS equivalent of ξ in DVCS. The curves show the same models as in Fig. 6.

Eq. (6) is expressed in terms of the Compton form factors:

$$\frac{1}{2}\sum_{\lambda,\lambda'}|M^{\lambda'-,\lambda-}|^2 = (1-\eta^2)(|\mathcal{H}_1|^2+|\tilde{\mathcal{H}}_1|^2) - 2\eta^2 Re(\mathcal{H}_1^*\mathcal{E}_1+\tilde{\mathcal{H}}_1^*\tilde{\mathcal{E}}_1) - (\eta^2+\frac{t}{4m_N^2})|\mathcal{E}_1|^2 - \eta^2\frac{t}{4m_N^2}|\tilde{\mathcal{E}}_1|^2\,. \tag{7}$$

Theoretical analyses [8, 10] have shown that the TCS cross section is smaller than the BH cross section for JLab 12 GeV kinematics, but like in DVCS, the BH and TCS amplitudes also interfere. When the initial-state photon is unpolarized, the interference term can be expressed as:

$$\frac{d\sigma_{\rm INT}}{dQ'^2\,dt\,d(\cos\theta)\,d\varphi} = -\frac{\alpha_{\rm em}^3}{4\pi s^2}\frac{1}{-t}\frac{M}{Q'}\frac{1}{\tau\sqrt{1-\tau}}\frac{L_0}{L} \times\Big[\cos\varphi\,\frac{1+\cos^2\theta}{\sin\theta}\,\Re e\tilde{M}^{--} - \cos 2\varphi\,\sqrt{2}\cos\theta\,\Re e\tilde{M}^{0-} + \cos 3\varphi\,\sin\theta\,\Re e\tilde{M}^{+-} + \mathcal{O}\Big(\frac{1}{Q'}\Big)\Big]\,, \tag{8}$$

where M is the proton mass. The variable τ,

$$\tau = \frac{Q'^2}{2(p\cdot q)} = \frac{Q'^2}{s-M^2}\,, \tag{9}$$

in TCS is the analog of the Bjorken variable $x_B = Q^2/(2p\cdot q)$ in DVCS. To leading twist accuracy,

$$\eta = \frac{\tau}{2-\tau}\,, \tag{10}$$

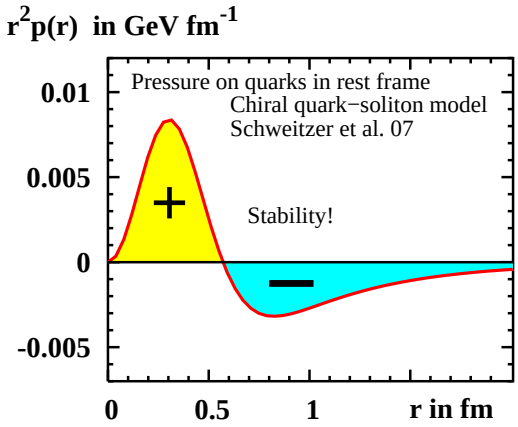

FIG. 8: Pressure experienced by quarks inside the nucleon calculated in the framework of the chiral quark-soliton model [21].

where η is given by Eq. (4). In Eq. (8), L_0 and L originate from the product of final-state lepton propagators [8] and $\tilde{M}^{\mu'\mu}$ are interference helicity amplitudes, where μ (μ') denotes the helicity of the incoming (outgoing) photon. In the handbag approximation, the photon (parton) helicity is conserved and, as a result, the only surviving contribution in Eq. (8) comes from $\tilde{M}^{--}$:

$$\tilde{M}^{--} = \frac{2\sqrt{t_0 - t}}{M} \frac{1-\eta}{1+\eta} \Big[F_1 \mathcal{H}_1 - \eta (F_1 + F_2) \tilde{\mathcal{H}}_1 - \frac{t}{4M^2} F_2 \mathcal{E}_1 \Big] , \tag{11}$$

where $-t_0 = 4\eta^2 M^2/(1-\eta^2)$ is the minimal momentum transfer at a given η (modulo $1/Q'^2$ corrections), and F_1 and F_2 are the Dirac and Pauli elastic form factors of the proton, respectively.

Unpolarized photons (from a helicity-averaged electron beam) give access to the real part of the CFFs. With a longitudinally polarized electron beam, producing circularly polarized photons with polarization $\nu \neq 0$, one can simultaneously study both the real and imaginary parts of the helicity amplitudes using the full expression for the interference term [8]:

$$\begin{aligned} \frac{d\sigma_{\rm INT}}{dQ'^2\, dt\, d(\cos\theta)\, d\varphi} \;=\; & -\frac{\alpha_{em}^3}{4\pi s^2} \frac{1}{-t} \frac{M}{Q'} \frac{1}{\tau\sqrt{1-\tau}} \frac{L_0}{L} \\ & \times \Big(\Big[\cos\varphi \, \frac{1+\cos^2\theta}{\sin\theta} \, \Re e \tilde{M}^{--} - \cos 2\varphi \, \sqrt{2} \cos\theta \, \Re e \tilde{M}^{0-} \\ & + \cos 3\varphi \, \sin\theta \, \Re e \tilde{M}^{+-} + \mathcal{O}\Big(\frac{1}{Q'}\Big) \Big] \\ & + \nu \Big[\sin\varphi \, \frac{1+\cos^2\theta}{\sin\theta} \, \mathrm{Im}\, \tilde{M}^{--} - \sin 2\varphi \, \sqrt{2} \cos\theta \, \Im m \tilde{M}^{0-} \\ & + \sin 3\varphi \, \sin\theta \, \mathrm{Im}\, \tilde{M}^{+-} + \mathcal{O}\Big(\frac{1}{Q'}\Big) \Big] \Big) , \end{aligned} \tag{12}$$

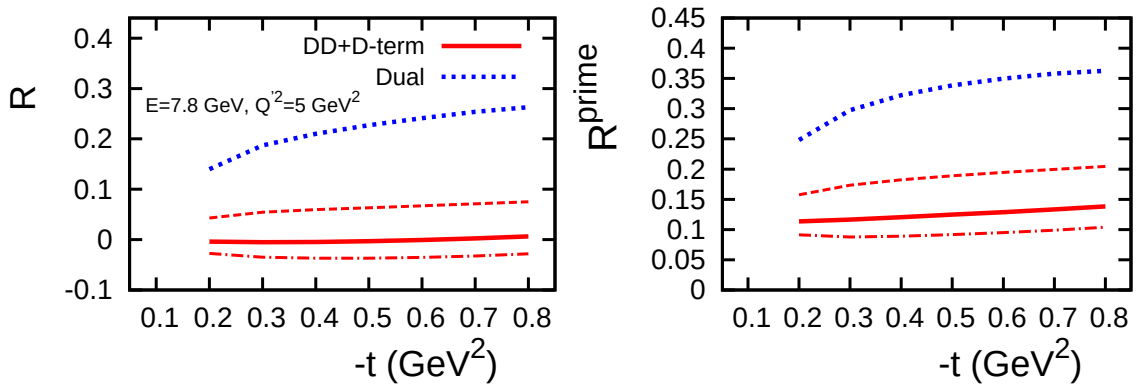

FIG. 9: Predictions for the cosine moment of the weighted cross section shown as a function of $-t$ at a fixed initial-state photon energy $E_\gamma = 7.8$ GeV and $Q'^2 = 5$ GeV^2. The curves correspond to GPD models based on the dual parametrization [13, 14, 15, 16] (blue) and the double distribution [17] (red), respectively. The three lower (red) curves correspond to different strengths of the D-term quantified by the parameter κ in Eq. (15). The moment R, defined in Eq. (14), is shown in the left panel, while the right panel shows the corresponding curves for R'. The latter is integrated over the θ-φ acceptance of CLAS12. The details are explained in Sect. 4. It is interesting to note the while the different integration contour changes the absolute value of R' compared with R, it does not diminish the sensitivity.

Under charge conjugation of the final-state lepton pair, which corresponds to the transformation $\varphi \to \varphi + \pi$, the TCS and BH cross sections are even, while the interference term is odd. This makes it possible to project out the TCS-BH interference through the weighted and θ-integrated cross section [8]:

$$\frac{dS}{dQ'^2\, dt\, d\varphi} = \int_{\pi/4}^{3\pi/4} d\theta\, \frac{L(\theta,\varphi)}{L_0(\theta)}\, \frac{d\sigma}{dQ'^2\, dt\, d\theta\, d\varphi}\,. \tag{13}$$

The contribution of, for instance, $\Re e\tilde{M}^{--}$, can now be obtained by taking the $\cos\varphi$-moment of S [8]:

$$R = \frac{2\displaystyle\int_0^{2\pi} d\varphi\, \cos\varphi\, \frac{dS}{dQ'^2\, dt\, d\varphi}}{\displaystyle\int_0^{2\pi} d\varphi\, \frac{dS}{dQ'^2\, dt\, d\varphi}}\,. \tag{14}$$

An example of the calculation of R as a function of $-t$ at a fixed initial-state photon energy $E_\gamma = 7.8$ GeV and $Q'^2 = 5$ GeV^2 is shown in the left panel of Fig. 9. The curves show predictions of calculations based on two GPD models: the dual parametrization [13, 14, 15, 16] (upper curve) and the double distribution [17] (lower three curves). The difference in the magnitude of R is quite significant, as would be expected given the difference in $\Re eH$ shown in Fig. 7. The three

lower curves correspond to different strengths of the D-term [2] in the double distribution, as quantified by the parameter κ in Eq. (15). It is interesting to note that for the standard value of κ, the double distribution predicts a cancellation with the D-term resulting in a small $\Re eH$ – a feature absent in the dual parametrization. The right panel in Fig. 9 shows the same calculations performed within the θ-φ acceptance of CLAS12. The details are explained in Sect. 4. In the calculations with the double distribution, for the GPD H we used:

$$H^q(x,\eta,t) = \int_{-1}^{1} d\beta \int_{-1+|\beta|}^{1-|\beta|} d\alpha \delta(x-\beta-\alpha\eta)\pi(|\beta|,\alpha) q(\beta,t) + \kappa \frac{1}{N_f}\Theta(\eta-|x|)D(x/\eta,t)\,, \quad (15)$$

where $\pi(\beta,\alpha)$ is the profile function that determines the degree of skewness, $q(\beta,t)$ is the off-diagonal quark parton distribution that reduces to the usual parton distribution in the $t=0$ limit, $D(x/\eta,t)$ is the D-term, and $N_f = 3$ is the number of active quark flavors. Note that we introduced the coefficient κ in front of the D-term to vary the strength of its contribution. For the D-term, we used the standard expansion in terms of the Gegenbauer polynomials $C_n^{3/2}$:

$$D(z,t=0) = -(1-z^2)(d_1\, C_1^{3/2}(z) + d_3\, C^{3/2}(z) + d_5\, C^{3/2}(z))\,. \quad (16)$$

The magnitude of the coefficients d_i in Eq. (16) was estimated in the chiral quark-soliton model at a low normalization scale [30]; QCD evolution to the needed values of Q'^2 somewhat decreases the values of the coefficients [3]. To test the sensitivity of R the D-term, we varied the parameter κ. The three curves in Fig. 9 correspond to $\kappa = 0.5$ (lower curve), $\kappa = 1$ (standard magnitude of the D-term), and $\kappa = 2$ (upper curve), respectively.

D. NLO corrections

It has been shown that the understanding of DVCS data needs higher order calculations for a reasonable extraction of GPDs to be possible [31, 32, 33]. This is even more likely to be the case for TCS. Indeed, TCS and DVCS amplitudes are identical (up to a complex conjugation) at lowest order in α_S, but differ at next-to-leading order, in particular because of the quite different analytic structure of these reactions [12]. The production of a timelike photon enables the production of intermediate states in some channels which are kinematically forbidden in the DVCS case. This opens the way to new absorptive parts of the amplitude. Experiments performed at JLab at 12 GeV will enable us to test the universality of GPDs extracted from DVCS and from TCS, provided that NLO corrections are taken into account.

Former experience with inclusive deep inelastic reactions teaches us that NLO corrections are likely to be more important in timelike reactions than in corresponding spacelike ones. The well-known example of the Drell-Yan K-factor teaches us that NLO corrections are more sizable in timelike processes, because of $i\pi$ factors coming from $log(-Q^2/\mu_F^2)$ terms. The importance

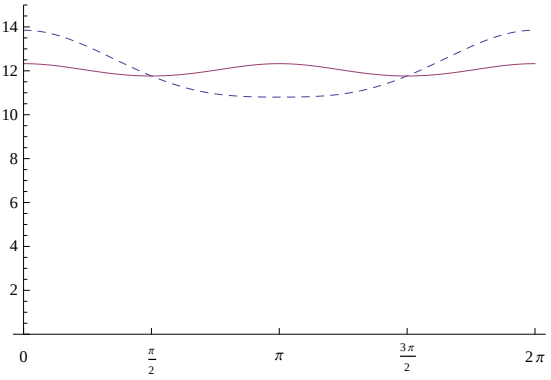

FIG. 10: NLO differential cross sections for Bethe-Heitler (solid) and Bethe-Heitler + Interference (dashed) terms as a function of φ, integrated over $\theta \in (\pi/4, 3\pi/4)$ for $E_\gamma = 11$ GeV, $Q^2 = 5$ GeV^2, $t = -0.1$ GeV^2 [34].

of next-order terms has also often been emphasized in the context of predictivity of theoretical calculations and proper choice of factorization scale [35]. The results for TCS should be indicative of other exclusive reactions with a timelike scale.

The symmetric part of the full amplitude of the general Compton scattering, in the factorized form is given by:

$$\mathcal{A}^{\mu\nu} = g_T^{\mu\nu} \int_{-1}^{1} dx \left[\sum_q^{n_F} T^q(x) F^q(x) + T^g(x) F^g(x) \right] , \tag{17}$$

where $T^{q,g}$ denote hard coefficient functions and $F^{q,g}$ quark and gluon GPDs. Coefficient functions for DVCS are well known [36, 37, 38, 39, 40] and for TCS were recently derived in [11]. It is convenient to express the amplitude (as for example in Ref. [8]) in terms of Compton form factors (CFF):

$$\mathcal{A}^{\mu\nu} = -e^2 \frac{1}{(p+p')^+} \, \bar{u}(p') \left[g_T^{\mu\nu} \left(\mathcal{H}\, \gamma^+ + \mathcal{E}\, \frac{i\sigma^{+\rho}\Delta_\rho}{2M} \right) \right] u(p), \tag{18}$$

which are defined in the following way:

$$\begin{aligned} \mathcal{H}(\xi,\eta,t) &= -\int_{-1}^{1} dx \left(\sum_q T^q(x,\xi,\eta) H^q(x,\eta,t) + T^g(x,\xi,\eta) H^g(x,\eta,t) \right) \\ \mathcal{E}(\xi,\eta,t) &= -\int_{-1}^{1} dx \left(\sum_q T^q(x,\xi,\eta) E^q(x,\eta,t) + T^g(x,\xi,\eta) E^g(x,\eta,t) \right) \end{aligned} \tag{19}$$

The question of the phenomenological consequences of the NLO corrections to Compton from factors for timelike Compton scattering is a topic of ongoing, intense theoretical study [11, 12].

It was shown that the real part of the CFF $\mathcal{H}$ is particularly sensitive to those corrections. This fact influences predictions for observables which depend on the interference term of the unpolarized cross section, *i.e.*, connected to the angular distribution of the lepton pairs in the angle φ (see the discussion in Sect. 2 C).

In Fig. 10 we show the BH and BH+interference term contributions to the $\gamma p \to e^+e^-p$ differential cross section [34] for $Q'^2 = 5$ GeV, $E_\gamma = 11$ GeV and $t = -0.1$ GeV^2 integrated over $\theta \in (\pi/4, 3\pi/4)$ as a function of the angle φ. Inclusion of NLO corrections also influences the ratio R defined by Eq. (14).

E. Amplitude analysis of Compton form factors

While the theory and phenomenology of exclusive processes and GPDs are now rather mature, the extraction of actual GPDs (Compton form factors) from available data is a complex problem that was started to be tackled only recently [9, 41, 42, 43, 44, 45, 46, 47, 48]. The complications include (i) generally low rates of exclusive processes, (ii) the limited number of independent experimental observables which are measured, (iii) the number of proton GPDs (at leading twist, the proton has four quark and four gluon parton helicity-conserving GPDs) (iv) which are themselves functions of four variables, and (v) the fact that even at the leading order, GPDs enter experimental observables in the form of convolutions with known kernels, which are called Compton form factors (CFFs). There are eight CFFs associated with the four quark helicity-conserving GPDs, namely $Re\{\mathcal{H}\}$, $Re\{\mathcal{E}\}$, $Re\{\tilde{\mathcal{H}}\}$, $Re\{\tilde{\mathcal{E}}\}$, $Im\{\mathcal{H}\}$, $Im\{\mathcal{E}\}$, $Im\{\tilde{\mathcal{H}}\}$, and $Im\{\tilde{\mathcal{E}}\}$.

The quasi model-independent CFF fitting procedure of Refs. [9, 43, 44, 45] has been implemented for the TCS process. The procedure simultaneously fits various experimental observables at a given kinematical point (*i.e.*, η, $|t|$, and Q'^2 for the TCS process), to the well-known leading-twist and leading-order TCS and BH amplitude,

This approach has been very successful for the DVCS process, allowing to extract, at the $\approx 30\%$ level, from various beam- or target-polarized observables, three CFFs ($Re\{\mathcal{H}\}$, $Im\{\mathcal{H}\}$, and $Im\{\tilde{\mathcal{H}}\}$) in JLab and HERMES kinematics [45]. For this procedure to be efficient, it is important to simultaneously fit several experimental observables; otherwise, fitting eight CFFs with only one observable makes the problem too under-constrained.

For this proposal, we have generated pseudo-data, at typical CLAS12 kinematics (E_e=11 GeV, Q'^2=4 GeV^2, and $-t$=0.2, 0.4, 0.6, and 0.8 GeV^2), for two TCS observables that we plan to extract: the unpolarized cross-section and the beam-polarized asymmetry. The CFFs used for the generation of the data were the VGG [49, 50] ones. Assuming different values for the experimental uncertainties on these two observables, we then fitted them and attempted to recover the generated CFFs. The results of the fit revealed a sensitivity to four CFFs: $Re\{\mathcal{H}\}$,

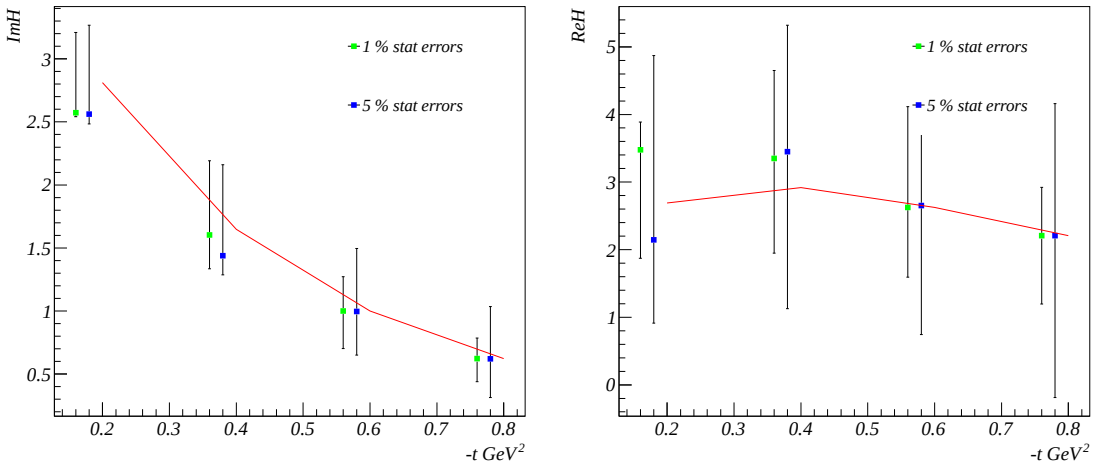

FIG. 11: *Left panel:* result on the extraction of the $Im\{\mathcal{H}\}$ CFF for E_e=11 GeV, Q'^2=4 GeV^2 and $-t$=0.2, 0.4, 0.6 and 0.8 GeV^2. *Right panel:* same for $Re\{\mathcal{H}\}$. Symbols and curves are described in the text.

$Im\{\mathcal{H}\}$, $Re\{\tilde{\mathcal{H}}\}$, and $Im\{\tilde{\mathcal{H}}\}$. Fig. 11 shows our result for $Re\{\mathcal{H}\}$ and $Im\{\mathcal{H}\}$, which are the most constrained. The red curve shows the generated CFFs and the blue and green points show the resulting fitted CFFs with their associated error bar, corresponding respectively to a 5% and a 1% uncertainty on the experimental cross section and asymmetry. A 1% uncertainty on the experimental observable is probably unrealistic but we nevertheless show the corresponding result as a "limit" and an "ideal" case. This figure show that with a realistic 5% experimental uncertainty, we should be able to extract the $Re\{\mathcal{H}\}$ and $Im\{\mathcal{H}\}$ CFFs with $\approx 60\%$ and 20% error, respectively. These resulting errors might appear rather large but we stress, firstly, that this fitting method is to a large extent model-independent and, secondly, that in this procedure, the error on the extracted CFFs is not directly proportional to the precision of the experimental data but rather reflects the influence (or our ignorance) of all the other CFFs. Precisely, we recall that the sub-dominant (kinematically suppressed) CFFs enter the fitting procedure and have an impact. Therefore, the errors on $Re\{\mathcal{H}\}$ and $Im\{\mathcal{H}\}$ in Fig. 11 reflect the "correlation" between all eight CFFs. Increasing the number of experimental observables to be fitted (for instance, using a longitudinally and/or a transversely polarized target) will strongly reduce the errors on the fitted CFFs and the number of CFFs to be extracted. In summary, the initial results presented in Fig. 11 demonstrate the general feasibility of extraction of GPDs from TCS data.

F. Comment on dispersion analysis

Dispersion relations provide a very powerful and model-independent method to relate the real and imaginary parts of scattering amplitudes based on such general properties as analyticity and crossing symmetry. For hard exclusive reactions, dispersion relations have been established and analyzed for DVCS, double DVCS (where the incoming photon has a spacelike virtuality and the outgoing photon is timelike), and for exclusive meson production [23, 24, 25].

For instance, for the CFF $\mathcal{H}^{q[+]}$ (the superscript [+] indicates the singlet combination corresponding to $q+\bar{q}$), one obtains the dispersion relation [24]:

$$\Re e\mathcal{H}^{q[+]}(\xi) = \frac{1}{\pi}\int_1^\infty d\omega \Im m C^{q[+]}(\omega)\int_{-1}^1 dx\left\{H^q(x,\frac{x}{\omega})\Big[\frac{1}{\omega\xi - x} - \frac{1}{\omega\xi + x}\Big] + \frac{2D^q(x)}{\omega - x}\right\}, \quad (20)$$

where $C^{q[+]}$ is the process-dependent hard-scattering kernel. The D-term enters the dispersion relation as a subtraction constant, *i.e.*, it gives an energy-independent contribution to $\Re e\mathcal{H}^{q[+]}$. The importance of the dispersion relation in Eq. (20) is that it quantifies the amount of information on GPDs that can be extracted from the real and imaginary parts of CFFs or, more generally, from amplitudes of exclusive processes. In addition, it provides a practical consistency check for models of GPDs. While dispersion relations for the TCS amplitudes have not yet been worked out, there should be no major difficulty in establishing them analogously to the cases that have already been considered.

G. Results from CLAS 6 GeV data

Our proposed 12 GeV experiment builds upon experience gained from the analysis of CLAS 6 GeV data. These pilot measurements demonstrated the feasibility of the experiment and allowed for the development of analysis methods suitable for CLAS. The 6 GeV data came from the e1-6, e1f, and g12 run periods. The first two are part of a CLAS Approved Analysis (CAA-DP09-01), the results of which have been documented in Ref. [51]. This analysis successfully used the same technique with quasi-real photons that we propose for the 12 GeV experiment, and demonstrated an impressive pion rejection of factor of 2.07×10^{-7} with three final-state particles detected (all except for the beam electron). Measuring the ϕ cross section in parallel with TCS showed that the flux of quasi-real photons is well understood. This analysis forms the basis of the current proposal. The g12 run period was the only high-energy CLAS data set with tagged real photons (up to 5.7 GeV) that utilized the Cherenkov counters. These had been made ready specifically for TCS and other e^+e^- physics. The analysis of the g12 data is ongoing. In addition to increasing the available statistics, the tagged-photon beam will make it possible to do an independent determination of the photon flux and offer an opportunity to explore event topologies with only two out of the three final-state particles detected.

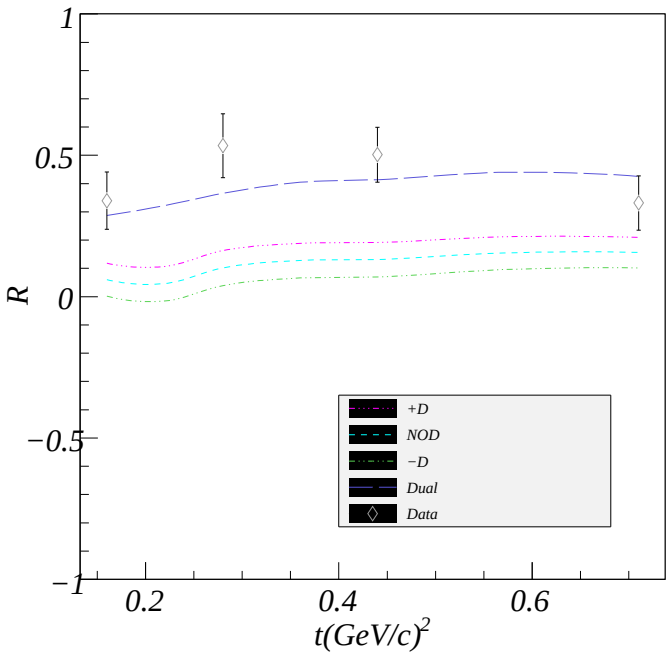

FIG. 12: The cosine moment of the weighted cross section, R', in the CLAS acceptance compared to GPD model calculations based on the dual parametrization [13, 14, 15, 16] (upper curve), and the double distribution [17] (lower curves) for three values of the D-term.

In addition to demonstrating the feasibility of the proposed measurement, the pilot experiments at 6 GeV stimulated the development of new analysis methods. An example of this was to use R' rather than R for the comparison with theoretical predictions. The two differ in the integration range in the $\varphi - \theta$ plane (the lepton c.m. angles φ and θ are defined in Fig. 3). Whereas R uses the ranges shown in Eqs. (13) and (14), R' introduces an acceptance function $a(\theta, \varphi)$ corresponding to the CLAS12 acceptance for a given kinematic bin. Using the same acceptance function for both the experimental and theoretical evaluations allows a straightforward comparison between data and model predictions. The difference between R' and R is discussed in more detail in Sec. 4 B together with the projected results.

Fig. 12 shows R' extracted from the combined e1-6 and e1f data sets for four bins in $-t$, compared with two GPD model calculations based on the dual parametrization [13, 14, 15, 16] and double distribution [17], respectively. Results from the latter are shown with three weights for the contribution from the D-term (+1, 0, and -1). Both the experimental and theoretical points were evaluated at the average value for the bin, but an event-by-event approach will be adopted in the future.

As useful as the 6 GeV experiments have been for the development of this program, the first true measurement of TCS will only be possible in the 12 GeV era, as the upgraded beam

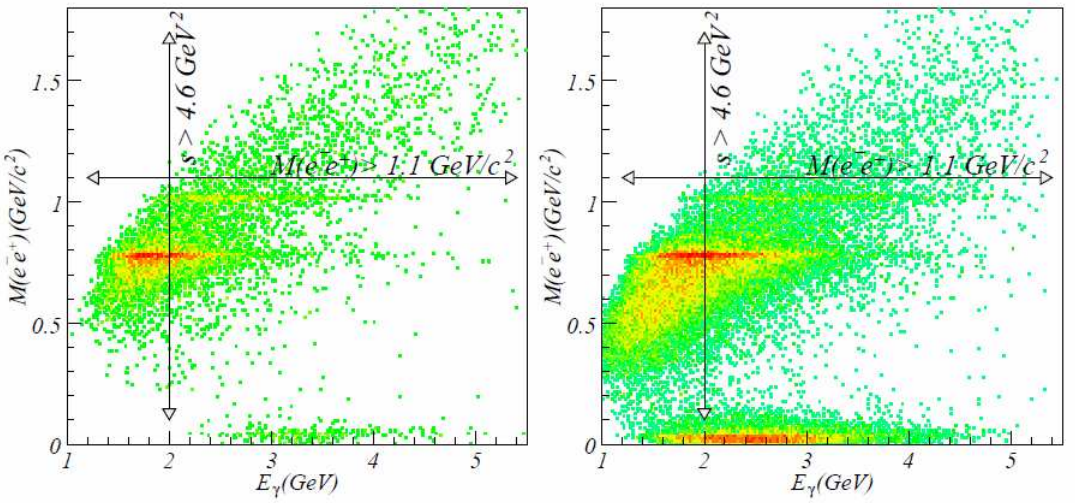

FIG. 13: e^+e^- invariant mass distribution vs. quasi-real photon energy for the e1-6 (left) and e1f (right) data sets. Only events with M_{ee} above the ϕ mass were used for the TCS analysis.

energy will make it possible to study a range of invariant lepton pair masses where there are no meson resonances that complicate the interpretation of the measurement. As shown in Fig. 13, only data above the ϕ mass were used for TCS analysis at 6 GeV, but at 12 GeV it will be possible to move this range above the mass of the ρ'. The increase in the luminosity of CLAS12 by an order of magnitude will, combined with a longer running time, also greatly improve the available statistics. And the higher beam energy will make it possible to probe higher values of s and Q'^2. Since the TCS equivalent of Bjorken x is $\tau = Q'^2/(s - M^2) \sim Q'^2/s$, an increase in s will also extend the coverage to lower τ (Bjorken x) at moderate values of Q'^2.

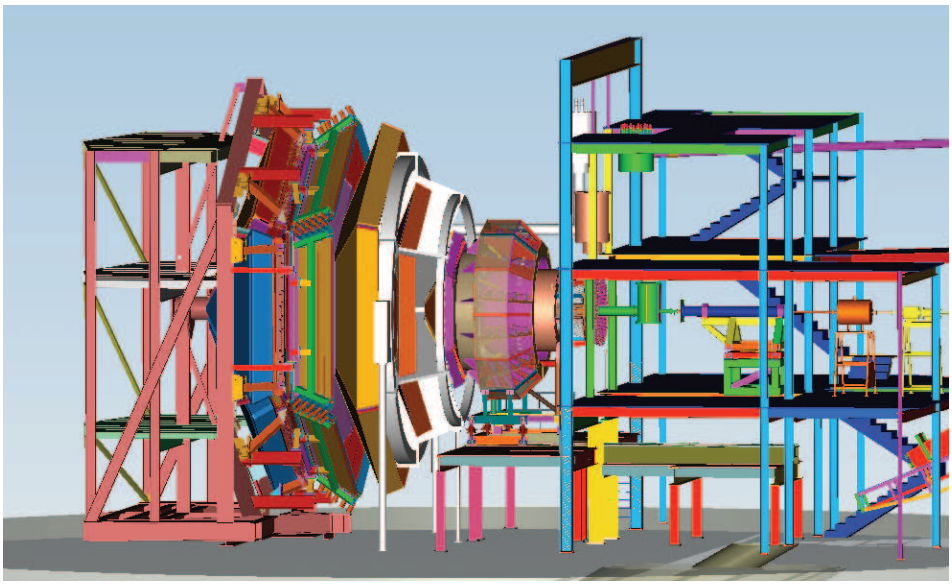

FIG. 14: The CLAS12 detector in Hall B.

3. EXPERIMENTAL SETUP

We propose to study photoproduction of lepton pairs, $\gamma p \to l^+ l^- p'$, in a wide range of kinematics using the CLAS12 detector in Hall B and a 11 GeV longitudinally polarized electron beam impinging on a hydrogen target. The analysis will use the fully exclusive electroproduction reaction:

$$ep \to e^+ e^- p'(e') \tag{21}$$

where the initial electron (e$'$) scatters at a small angle ($\sim 0^\circ$), and escapes detection in CLAS12. In Eq. (21), e^+e^- is the produced lepton pair, and p' is the recoil proton. The main goal of the measurement is to extract cosine and sine moments of the weighted cross section, and the four-fold differential cross section:

$$\frac{d^4\sigma}{dQ'^2 dt d\cos\theta_{CM} d\varphi_{CM}} \tag{22}$$

for several bins of $s = (q^\mu + p^\mu)^2$, $t = (p'^\mu - p^\mu)^2$, $Q'^2 = (e_1^\mu + e_2^\mu)^2$, and the electron polar and azimuthal angles θ_{CM} and φ_{CM} in the (e$^+$e$^-$) Center-of-Mass system, respectively. Here $q^\mu = k^\mu - k'^\mu$, with k^μ (k'^μ) being the initial (scattered) electron four-momentum vector, p^μ (p'^μ) is the target (recoil) proton four vector, and e_1^μ and e_2^μ are four-momenta of the produced e^+ and e^-. The momentum of the scattered beam electron, k', will be deduced from missing momentum analysis.

Parameters	Forward Detector	Central Detector
Charged tracks:		
polar angular range (θ)	5° to 35°	35° to 125°
resolution:		
polar angle ($\delta\theta$)	< 1 mr	< 10 mr to 20 mr
azimuthal angle ($\delta\phi$)	< 4 mr	< 5 mr
momentum (δp/p)	$< 1\%$ at 5 GeV/c	$< 5\%$ at 1.5 GeV/c
Neutral particles:		
angular range (θ)	5° to 40°	40° to 125° (neutrons)
angular resolution ($\delta\theta$)	< 4 mr	< 10 mr
Energy resolution	$< 0.1/\sqrt{(E)}$	$< 5\%$
PID:		
e/π	full momentum range	NA
π/p	full momentum range	< 1.25 GeV/c
K/π	< 3 GeV/c	< 0.65 GeV/c
K/p	< 4 GeV/c	< 1 GeV/c

TABLE I: CLAS12 design characteristics.

This final state contains an electron that will provide a standard CLAS12 electron trigger. The data can thus be collected in parallel with any CLAS12 electroproduction experiment. The base equipment and DAQ of CLAS12 are suitable for conducting these measurements. Identification of quasi-real photoproduction of e^+e^- pairs will be based on the detection of the final-state particles, and a missing-momentum analysis of the undetected beam electron, performed in a similar manner as in the TCS analysis of the CLAS 6 GeV data [51].

A. The CLAS12 detector

As part of the 12-GeV upgrade, the CLAS detector [52] in Hall B will be upgraded to CLAS12 [53]. The CLAS12 detector, shown in Fig. 14, is designed to carry out experiments using high energy electron beams incident on polarized and unpolarized targets at luminosities up to $L = 10^{35}$ cm^{-2} sec^{-1}. CLAS12 consists of two parts, the forward detector (FD) and the central detector (CD). The design characteristics of CLAS12 are presented in Table I. Particles in CLAS12 will be detected and identified by measuring their momenta, time-of-flights, number of photons produced in threshold Cherenkov counters, and energy losses in the calorimeters and scintillator counters.

The forward detector will be able to detect and identify charged and neutral particles scattered between 5° and 35° over the full momentum range. Particles will be detected in six identical magnetic spectrometers based on a six-coil, superconducting toroidal magnet. Each spectrom-

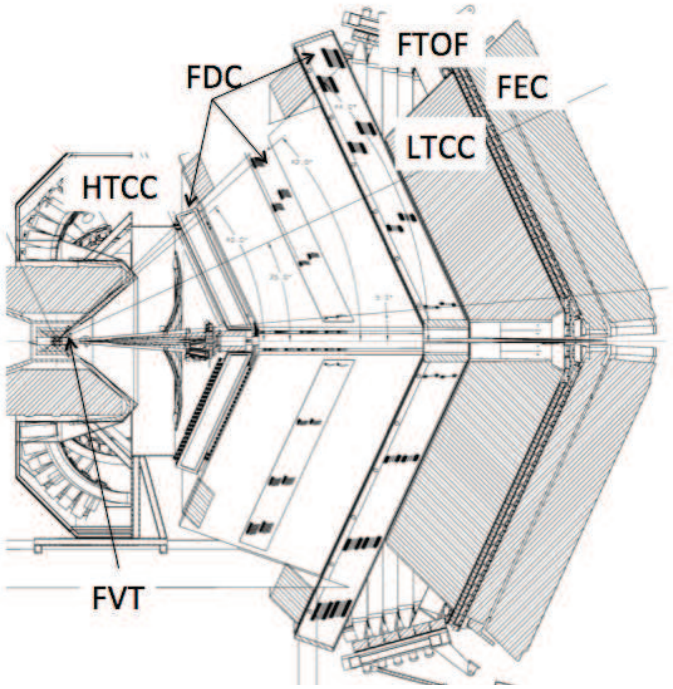

FIG. 15: Mid-plane view of the CLAS12 forward detector.

eter (sector of the forward detector) will be equipped with a forward vertex tracker (FVT), a high-threshold Cherenkov counter (HTCC), a set of drift chambers (FDC), a low-threshold Cherenkov counter (LTCC), scintillation counters (FTOF), and electromagnetic calorimeters (FEC) as shown in Fig. 15. Trajectories of charged particles, and hence their momenta and path lengths, will be measured using the FDC. The FVT will be based on micromega detectors and will be mounted $\sim$ 25 cm downstream of the solenoid center (also the target center). The vertex tracker will allow accurate reconstruction of the track parameters at the production vertex in a presence of the high longitudinal magnetic field of the solenoid. Planes of scintillator counters with $\sim$ 80 ps time resolution form a forward time-of-flight system, the FTOF. The time measured in the FTOF will be used for charged hadron identification, together with the path length and momentum measured in the FDC. Two threshold Cherenkov counters, the HTCC with a CO_2 radiator giving a pion momentum threshold of 4.9 GeV/c, and the LTCC with a C_4F_{10} radiator and a pion momentum threshold of 2.7 GeV/c, will be used to identify electrons and high-momentum charged pions. Forward electromagnetic calorimeters will be used to measure the energy of showering particles (e^-, γ) and the time of the hit. The FEC is a sampling calorimeter with transverse and longitudinal segmentation of the light readout system. Transverse segmentation will allow to determine the hit position with $\sim$ 1 cm accuracy, and to

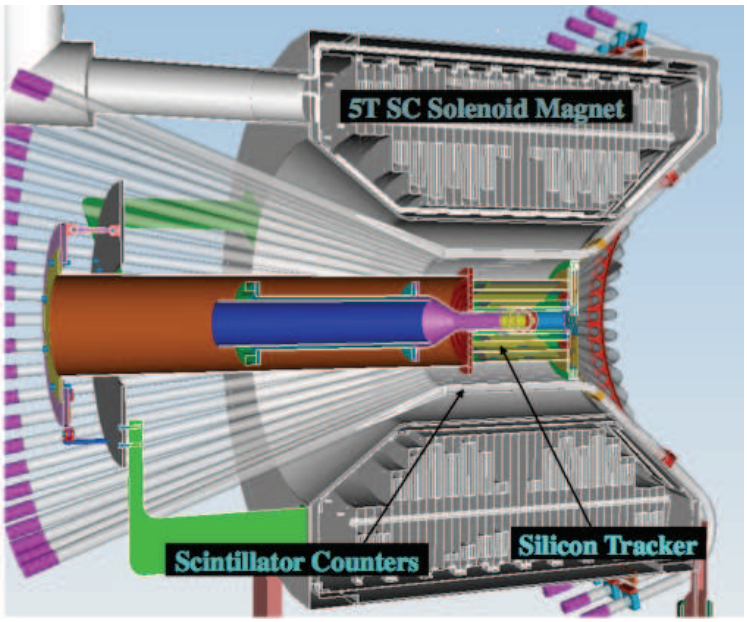

FIG. 16: Rendering of the CLAS12 central detector.

separate close lying showers (*e.g.*, from high-energy $\pi^0 \to \gamma\gamma$ decay). The longitudinal segmentation will help in e/π separation. The FEC is also the main detector in the forward region of the CLAS12 used for neutron detection.

The CD is based on a 5T superconducting solenoid magnet and consists of a barrel tracker and a time-of-flight system. The solenoid magnet will also serve as shielding from Möller electrons for the FD. The CLAS12 target system will be located in the center of the CD. The central detector will detect charged hadrons and neutrons with momenta below 1.5 GeV/c in an angular range from 37° to 125°. Charged particles will be detected by two barrel-shaped detectors, a Si-tracker (BST) and time-of-flight counters (CTOF), as shown in Fig. 16. Both detectors are positioned inside the solenoid magnet and cover the full azimuthal angular range. The BST will measure the momentum of charged tracks with better than 5% momentum resolution. The CTOF will measure the time-of-flight of charged particles with 60 ps time resolution. As mentioned above, there will be a neutron detector positioned between the CTOF and the cryostat of the solenoid.

CLAS12 will have a free-running DAQ system. Flash ADCs and TDCs will collect data in pipeline mode. Readout of data will be performed after the trigger decision is made. The expected event readout rate is 10 kHz.

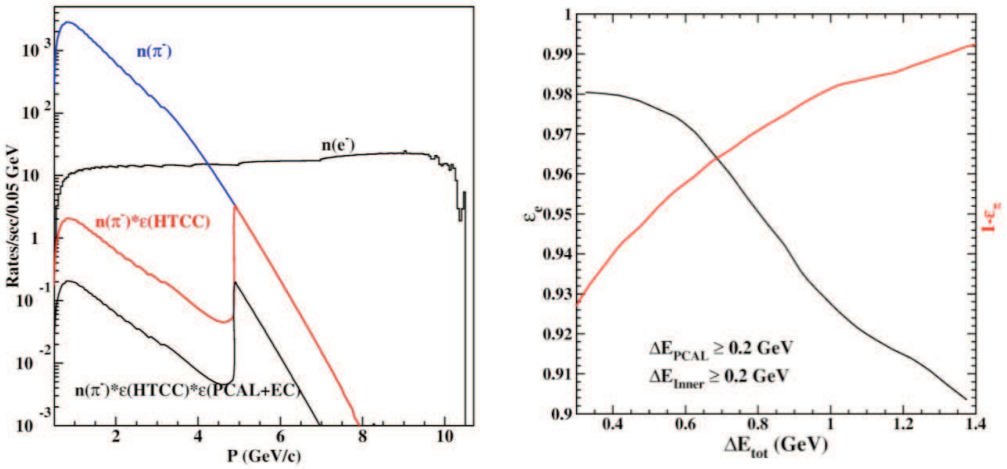

FIG. 17: Electron identification in the FD. *Left panel:* The red line shows the pion suppression at using only the HTCC (it merges with the pion line above the pion threshold). The lower black line is the includes the additional pion suppression from the FEC expected at the trigger level. In offline analysis, the suppression factor in the FEC can be increased to 100. *Right panel:* Electron efficiency vs. pion suppression factor for momenta > 4.9 GeV/c where only the fractional energy deposited in the FEC is used for electron ID.

B. Particle identification

The CLAS12 particle identification (PID) system has three components; electron identification, charged hadron identification (p, $\pi^{\pm}$, $K^{\pm}$), and neutral particle identification (n, γ). Electrons and photons will be detected and identified in the FD, and charged hadrons and neutrons in both the FD and the CD. The measurements in this proposal require clean identification of electrons, positrons, and protons.

Electron identification is the most important component of the PID for the CLAS12 experiments, and the proposed experiment in particular. Reliable electron ID is required not only for offline analysis, but also at the trigger level. Using a coincidence of the signals from the HTCC and the FEC, single pions will be suppressed by more than four orders of magnitude. Electrons with momenta below 4.9 GeV/c will be identified using the photoelectron statistics in the HTCC and the fractional energy deposition in the FEC. Above 4.9 GeV/c only the FEC will be used.

Fig. 17 shows the electron/pion separation. In the left panel rates of negatively charged pions and electrons are shown as a function of momentum. With a 3 *p.e.* cut, the HTCC provides a pion suppression of 2×10^3. If needed, this cut can be placed higher (by up to a factor of two) with a small loss in electron efficiency. The FEC can provide another factor of 10

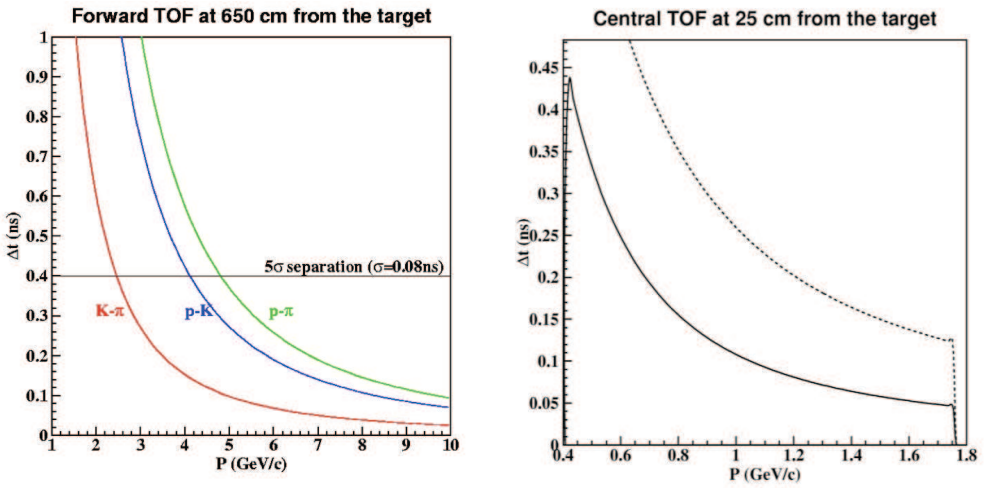

FIG. 18: Charged hadron ID. The left graph shows the time difference vs. momentum for kaons and pions (red), protons and kaons (blue), and protons and pions (green). The right graph shows the same dependence for kaons and pions (solid line) and protons and kaons (dashed line).

pion suppression at the trigger level. However, as shown by GEANT simulations of the FEC, a pion suppression in excess of a factor of 100 can be reached by using both the transverse and longitudinal distributions of the shower in offline analysis. The combination of FEC and HTCC is then expected to give a suppression of at least 2×10^5 for single charged pions.

Charged-hadron identification in both the FD and the CD will rely on momentum and time measurements. The time difference between different particle species is shown in Fig. 18 as a function of momentum. The FTOF, with a time resolution of 80 ps and an average path length of $\sim$ 650 cm from the target to the FTOF plane, will allow 5σ p/K separation for momenta below 4 GeV/c, and p/π separation for momenta below 5 GeV/c (see the left graph of the figure). The CTOF time resolution will be 60 ps. This will allow p/K separation up to 1.2 GeV/c, as shown by solid and dashed lines, respectively, in the right graph of Fig. 18.

C. Detection of exclusive e^+e^- events

To study the CLAS12 performance for the proposed measurements, simulations were carried out using the CLAS event generator FSGEN [54]. The e^+e^-p events were generated over a wide range of kinematics. Each event was weighted by the relevant cross section. For the Bethe-Heitler (BH) events, the cross section from Ref. [55] was used. The kinematics of the scattered electron were defined with a $\frac{1}{Q^4}$ dependence. The response of the detector was simulated using the CLAS12 Fast Monte Carlo (FASTMC) algorithm [56].

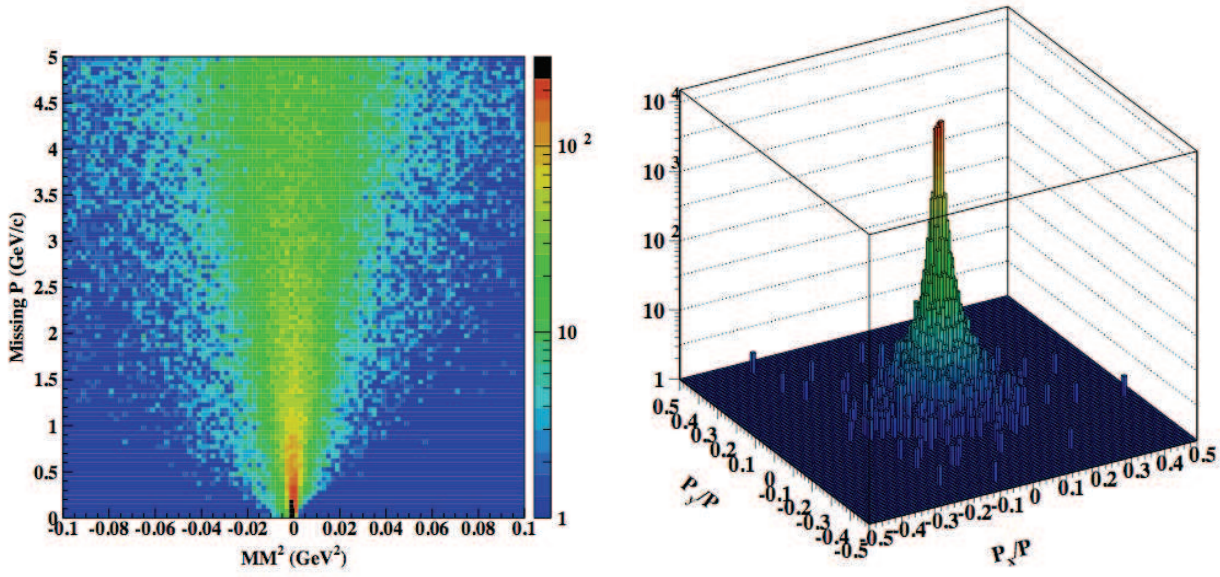

FIG. 19: *Left panel:* Distribution of missing momentum vs. missing mass squared in the reaction $ep \to e^+e^-p'(e')$. *Right panel:* Distribution of the x and y components of the missing momentum.

Fig. 19 shows the missing mass and missing momentum distributions (left), and transverse components of the missing momentum (right) for simulated e^+e^- electroproduction events. The CLAS12 momentum- and angular resolution is sufficient for a clean selection of quasi-real photoproduction events, where the beam electron scatters at very forward angles ($P_x/P \sim 0$, $P_y/P \sim 0$, and MM ~ 0).

Fig. 20 shows the kinematics of electrons and positrons for BH events detected in CLAS12. As was discussed above, electrons will be detected and identified in the forward detector, where the polar angle of detection is limited to the range between 5° and 35°. In this range, the electrons and positrons have momenta from 1 GeV/c to 10 GeV/c, but as shown in the center panel of Fig. 20, only a few percent of events have both leptons with momenta above the HTCC pion threshold. These pairs can be removed from analysis with a small loss of statistics. The remaining pairs will have suppression factors of 2×10^7 if one lepton has a momentum below the HTCC pion threshold, or in excess of 10^{10} if both lepton momenta are below 4.9 GeV/c.

The kinematics of protons in exclusive e^+e^- events are shown in the right panel of Fig. 20. The momenta and angles are in the comfort zone for p/K and p/π separation using the time-of-flight systems in the FD and the CD.

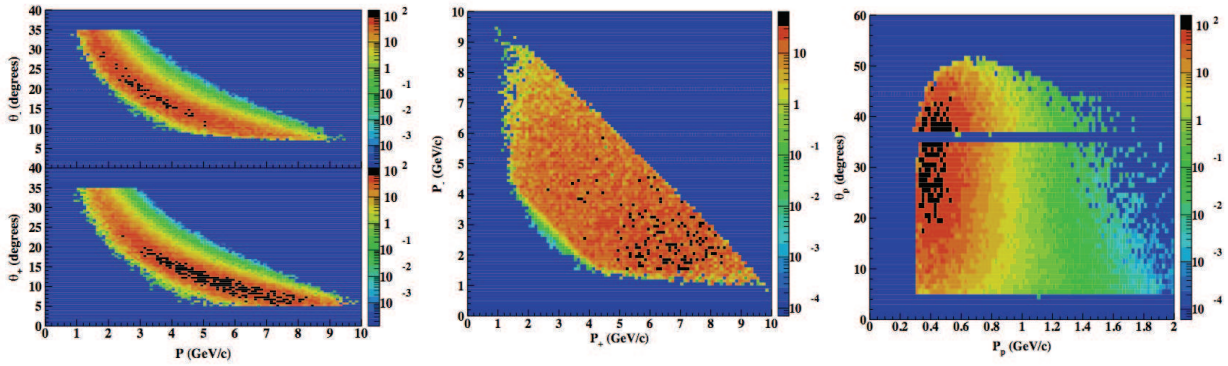

FIG. 20: *Left panel:* Electron and positron kinematics for TCS events with $Q'^2 > 2$ GeV^2 accepted in CLAS12. *Center panel:* momentum of electrons vs. momentum of positrons. Almost always one lepton has a momentum below 4.9 GeV/c. *Right panel:* Kinematics of protons from TCS events with $Q'^2 > 2$ GeV^2 accepted in CLAS12.

4. PROJECTED RESULTS FOR TCS

sIn this section we describe the projected uncertainties for cross sections and moments of weighted cross sections for representative kinematics. Acceptances and rates are discussed as well. Unless stated otherwise, the nominal CLAS12 electron luminosity of $L = 10^{35}$ cm^{-2} sec^{-1} is assumed. The 120 days already approved by the PAC for running with the standard setting of the torus field, 80 at full and 40 at reduced luminosity, have been approximated by 100 days at full luminosity. The proposed additional 30 days of running with a reversed torus field will add to the statistics.

A. Acceptance

The simulation and selection of exclusive e^+e^-p events was discussed in Sect. 3 C. The resulting acceptance is shown in Fig. 21 as a function of the lepton invariant mass squared, ($M^2_{e^+e^-} = Q'^2$), and the four-momentum transfer $-t$ for four bins in the c.m. energy squared s between 13.5 and 21.5 GeV^2 (corresponding to E_γ from 6 to 11 GeV), each with a width of 2 GeV^2. As shown in the left panel of Fig. 20, in this range of incident photon energies, the lab-frame opening angle is quite large, and the angular distribution of lepton pairs with invariant masses $M^2_{e^+e^-} > 2$ GeV^2 is well matched to the CLAS12 acceptance. The middle panel further shows that only for a few percent of the events will both leptons have lab momenta above 4.9 GeV, which means that the high-threshold Cherenkov counter (HTCC) can be used to enhance the PID efficiency of the forward electromagnetic calorimeter (FEC) for at least one of the

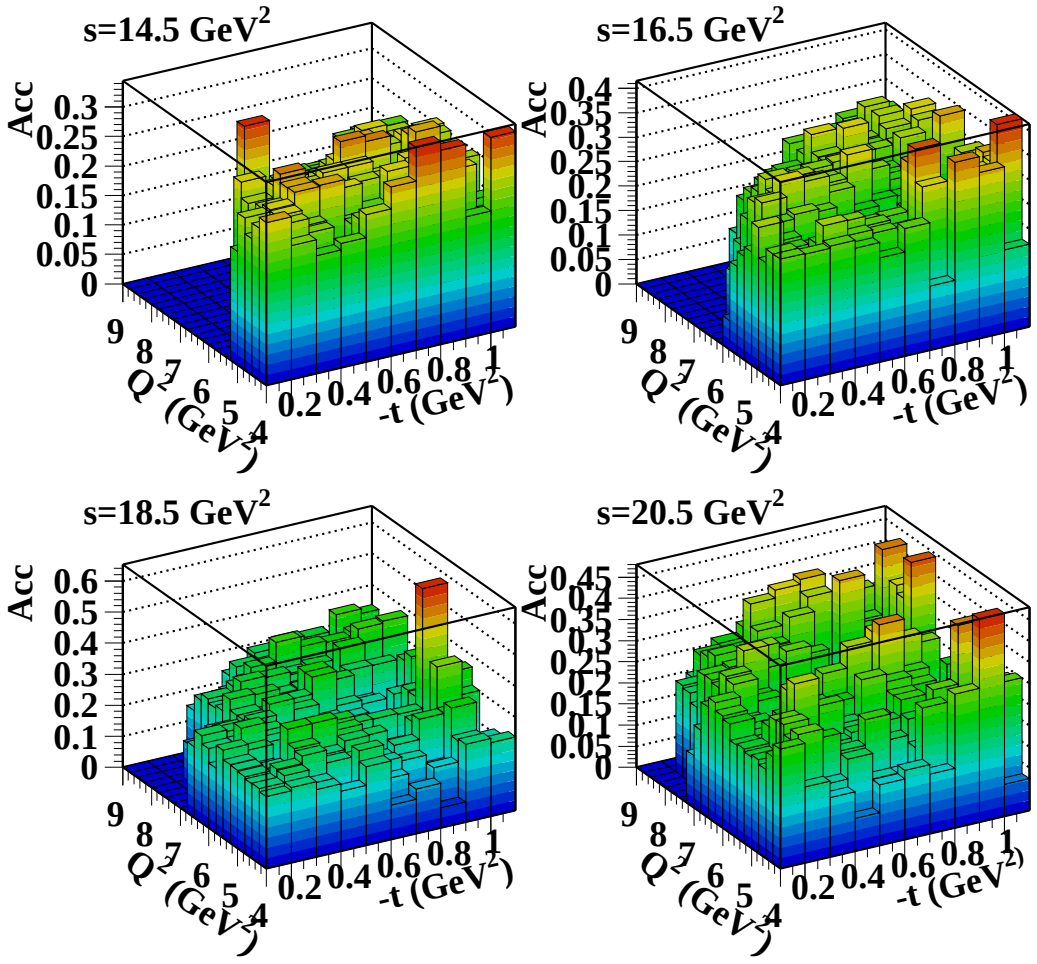

FIG. 21: CLAS12 acceptance for BH events in the reaction $ep \to e^+e^-p'(e')$ showing the accessible ranges of Q'^2 and $-t$ for four bins of s.

leptons. Measuring the exclusive reaction $ep \to e^+e^-p'(e')$ also requires detection of the recoil proton. The proton kinematics are shown the right panel of Fig. 20. These are also well matched with the CLAS12 acceptance for a wide range in $-t$.

The TCS acceptance in the θ_{CM} vs. φ_{CM} plane is shown in Fig. 22. Please note that the TCS angles defined in Fig. 3 are here explicitly written with an index CM, referring to the lepton Center-of-Mass frame. Generated e^+e^-p events are shown in the left panel, while accepted events for four bins in $-t$ are shown in the right panel.

The (unprimed) expressions for the moments of the weighted cross section, such as R

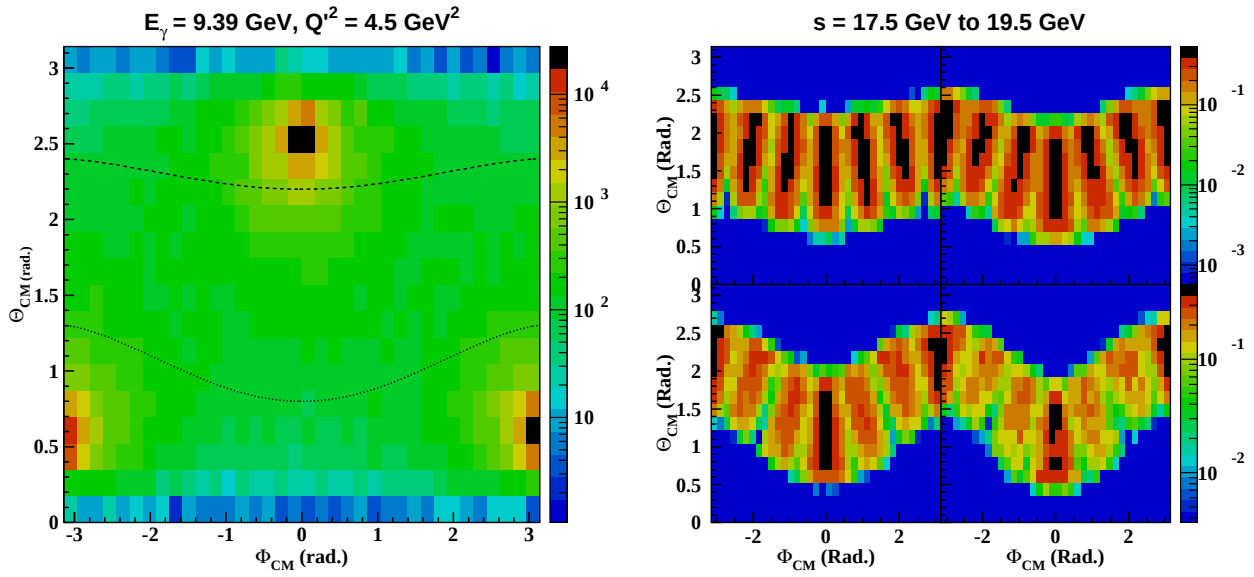

FIG. 22: *Left panel:* Distribution of generated e^+e^- events in the θ_{CM} vs. φ_{CM} plane for a bin centered at $-t = 0.3$ GeV^2, $Q'^2 = 4.5$ GeV^2, and $E_\gamma = 9.39$ GeV^2. The curve shows the limits of the CLAS12 acceptance for these kinematics. *Right panel:* Accepted events shown for four 0.2 GeV^2-wide bins in $-t$, centered at 0.2, 0.4, 0.6, and 0.8 GeV^2, respectively, in a bin of s ranging from 17.5 to 19.5 GeV^2.

defined in Eqs. (13) and (14), are first integrated over θ_{CM} and then independently over φ_{CM}. In this section we will use primed moments that can be more easily compared with the experimental data. These are instead integrated over a band in the θ_{CM} vs. φ_{CM} plane defined through a φ_{CM}-symmetric acceptance function $a(\theta_{CM}, \varphi_{CM})$. This function is chosen such that it coincides with the envelope of the CLAS12 acceptance for each bin. Thus, the experimental and calculated values of R' are defined in a consistent way. Still, while the CLAS12 acceptance does not influence the comparison between data and theory at the level of the contour of integration in the θ_{CM} vs. φ_{CM} plane, the experimental yields have to be corrected for acceptance. As is the case with all cross section measurements in CLAS, this correction is done through simulations, for which the standard CLAS12 package GEMC will be used. Since the incoming and outgoing photons are generally not collinear (and the beam line does not lie in the lepton decay plane), the six coils of the CLAS12 torus magnet do not appear as holes with no events in the φ_{CM}-distribution as they do for φ_{lab}, but the coils do create φ_{CM}-regions where the acceptance is small. The uncertainties in the acceptance corrections can be further reduced through experimental studies of the detector performance. This is discussed further in section 5 C.

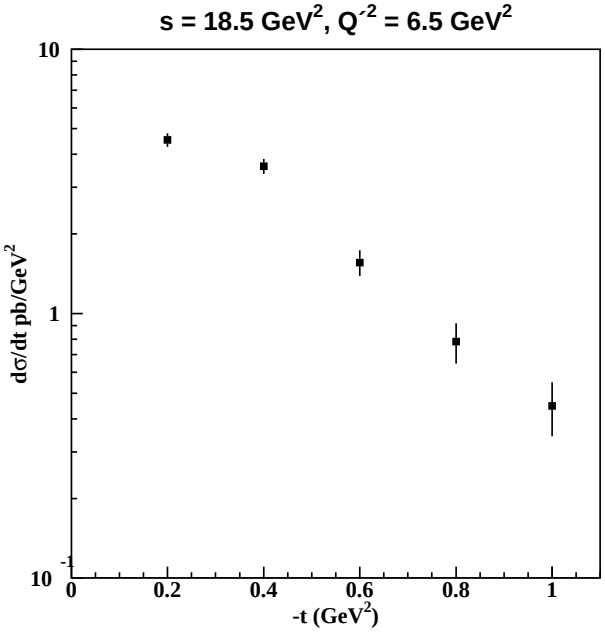

FIG. 23: Differential cross section as a function of the four-momentum transfer, integrated over φ_{CM} and θ_{CM} for a bin in s from 17.5 to 19.5 GeV^2 and Q'^2 from 6 to 7 GeV^2. The error bars on the points correspond to 100 days of running.

B. Projected results

Since the TCS cross section will not be measured separately but in combination with the larger BH cross section with which it interferes, the rate estimates for TCS were based on the BH cross section as given in Ref. [57]. As an example, the statistical uncertainties in the cross section measurements for one bin in s and Q'^2 is shown in Fig. 23 for 100 days of running.

The results from the TCS analysis will come in the form of the measured differential cross section and cosine and sine moments of the weighted cross section. The cross section measurement will constrain global fits of Compton form factors (CFFs), and could be used for extraction of helicity amplitudes, which are related to the CFFs through Eq. (11), by fitting the data in the CLAS12 θ_{CM}-φ_{CM} acceptance. The cosine and sine moments are also directly related to the helicity amplitudes (and hence CFFs and GPDs). A comparison of the moments evaluated within the CLAS12 acceptance imposes strong constraints on GPD models, and in particular their predictions for the real part of the amplitude. Since the global fits will eventually be constrained not only by TCS data, but also data from other exclusive channels (and perhaps theory), the final impact of each channel on the global fit result is *a priori* difficult to quantify, but initial fits using only simulated TCS data, shown in section 2 E, demonstrate the feasibility

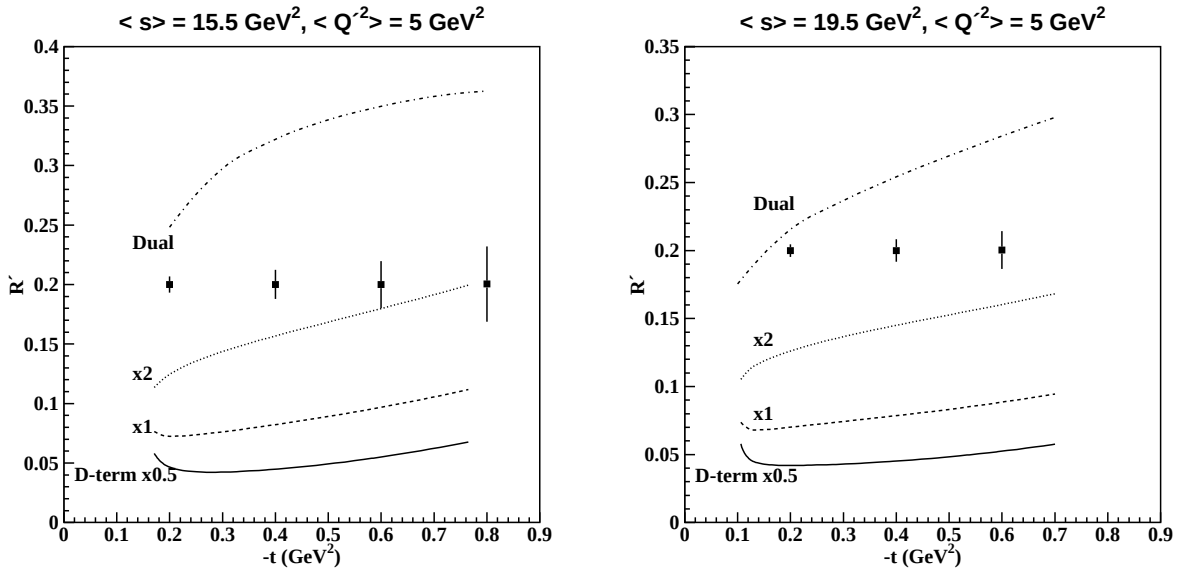

FIG. 24: The cosine moment of the weighted cross section, R', obtained through φ_{CM}-dependent θ_{CM} integration, shown as a function of the four-momentum transfer $-t$, in a bin of Q'^2 centered at 5 GeV^2. Each of the four t-bins has a width of 0.2 GeV^2. The left panel shows a bin in s centered at 15.5 GeV^2, while the right panel shows a bin at 19.5 GeV^2. The upper curve shows a GPD model calculation based on the dual parametrization [13, 14, 15, 16], while the lower ones were based on the double distribution [17] with different weights applied to the D-term contribution. The solid, dashed, and dotted lines correspond to weights of 0.5, 1.0, and 2.0, respectively. The error bars on the points correspond to 100 days of running. The points are placed arbitrarily at $R' = 0.2$.

of this approach.

The experimental sensitivity of the proposed measurement is easiest to evaluate through the moments. The cosine moment R', related to $\Re e\tilde{M}^{--}$, will be used as an example. In the extraction of the moments, the angles φ_{CM} and θ_{CM} are integrated over, and only the kinematic variables $-t$, s, and Q'^2 remain (although the latter two are directly related to τ and η, which are the TCS equivalents of x_B and ξ in DVCS). In order to understand if factorization holds, the Q'^2-dependence will initially be studied in relatively narrow bins (~ 1 GeV^2). However, for the final extraction of R', wider bins in Q'^2 can be used. Since this experiment is not directly aimed at spatial imaging, the t-dependence of the moments is only one of the dependencies that will eventually be studied. Nevertheless, it serves as a good example of the sensitivity of the experiment to various GPD models and their features.

The projected statistical uncertainties for R' are shown in Fig. 24 for 100 days of running for two bins in s centered at 15.5 and 19.5 GeV^2, respectively, in a bin of Q'^2 centered at 5 GeV^2.

This is the lowest wide Q'^2-bin in the primary range of interest (*i.e.*, the range between 4 and 9 GeV^2), where the statistics will be the highest. Since $\tau = Q'^2/(s - M^2)$, the two s-bins shown in Fig. 24 correspond to average values of τ of 0.34 and 0.27, respectively. Higher values of τ (or Bjorken x) can be reached at higher Q'^2 or lower s, but with poorer statistics. Nevertheless, the fact that the kinematic reach in τ is not constrained by an external mass Q^2, but only the ratio of $Q'^2 = M_{e^+e^-}$ and s makes it relatively easy to probe the τ-dependence if the data are re-binned accordingly. In addition to the points with the projected statistical uncertainties, Fig. 24 also shows two sets of curves. The upper one corresponds to a calculation of R' using the dual parametrization [13, 14, 15, 16], while the lower three are based on the double distribution [17] with different weights κ applied to the D-term contribution (0.5, 1.0, and 2.0, respectively). The D-term can be calculated within the framework of the dual parametrization, but it does not appear as an independent quantity that can easily be varied. Since the calculations indicate that the Q'^2-dependence for the D-term is relatively small, the bins with highest statistics (*i.e.*, the lowest Q'^2) are of greatest interest for this study.

While the absolute value of R' can differ somewhat from that of R, an example of which was shown in Fig. 9, this does not reduce its sensitivity to $\Re e\tilde{M}^{--}$ or GPD model predictions, nor does it pose a significant complication for the interpretation. The difference is caused by the fact that when integrated over the CLAS12 acceptance, defined by the φ_{CM}-symmetric acceptance function $a(\theta_{CM}, \varphi_{CM})$, the BH contribution is not zero. The BH contribution can, however, be treated exactly in the theoretical calculation to which the experimental result is compared. The shift is also relatively small, which is not surprising given that the CLAS12 acceptance is generally at least as restrictive as the range of $\pi/4 < \theta_{CM} < 3\pi/4$ used for the integration in Eq. (13), chosen to exclude regions where BH is very large. Additional θ_{CM}-cuts can also easily be imposed if that would prove advantageous.

In conclusion, the comparisons in Fig. 24 show that the sensitivity of the proposed measurement makes it possible to differentiate between different D-term contributions using the bins with the highest statistics (*i.e.*, the ones at the lower end of the Q'^2-range), while discrimination between different GPD models/parametrizations can be done over the full range in Q'^2. It is, however, worth keeping in mind that this will be the first true measurement of the timelike Compton process, and as such can bring new insights beyond the ability to discriminate between model predictions.

5. J/ψ CROSS SECTION NEAR THRESHOLD

As stated in our Letter of Intent (LOI11-106), this proposed e^+e^- experiment will also measure the cross section of J/ψ photoproduction on the proton near threshold ($E_{\gamma,\text{threshold}} = 8.21$ GeV). Since a first experimental extraction of the J/ψ photoproduction cross section is relatively straightforward, this measurement is expected to be one of the first results from CLAS12. J/ψ production near threshold is a rich and complex physics topic in its own right and presently the subject of intense theoretical research. The physics of J/ψ production near threshold with CLAS12 will be described in a separate proposal, which will include also electroproduction and measurements with nuclear targets. In the context of the present TCS proposal, measurement of the J/ψ photoproduction cross section is of great interest for the purpose of a precise yield extraction. The projected results would, however, represent a dramatic improvement over the world data on J/ψ production near threshold, and would thus impact the on-going theoretical discussions. In this section we briefly describe the current understanding of J/ψ production near threshold, the projected results, and the role of the J/ψ measurement in the present TCS experiment.

A. J/ψ production near threshold

The production of heavy quarkonia and their interaction with hadronic matter are key questions of QCD, which are being studied through production experiments at different energies and various theoretical approaches; see Ref. [58] for a recent review. Because of the small spatial size of heavy quarkonia on the hadronic scale, $r_{Q\bar{Q}} \ll 1$ fm, one can use QCD operator methods to describe their interactions with hadrons and external probes in controlled approximation. Heavy quarkonium production probes the local color (gluon) fields in the nucleon, and can reveal properties such as their response to momentum transfer, their spatial distribution, and their correlation with valence quarks. The dynamics that produces the relevant gluon fields in the nucleon changes considerably between high energies and the near-threshold region, creating a fascinating landscape that calls for detailed experimental study. At high energies ($W > 10\,\text{GeV}$) exclusive J/ψ photo– and electroproduction probes the nucleon's gluon GPD at small momentum fractions $x \sim M^2_{J/\psi}/W^2 \ll 1$ and can be used to infer the transverse spatial distribution of small–x gluons in the nucleon; see Ref. [59] for a review; such experiments were performed at HERA [60, 61] and FNAL [62], and a detailed program of "gluon imaging" along these lines is planned with a future Electron Ion Collider (EIC) [63]. In exclusive J/ψ production near threshold, the minimum invariant momentum transfer to the nucleon becomes large: $|t_{\text{min}}| = 2.23$ GeV^2 at threshold, and $|t_{\text{min}}| = 1.3 - 0.4$ GeV^2 in the $E_\gamma = 8.5 - 11$ GeV range. The process is therefore analogous to elastic eN scattering at large $|t|$, only that the "probe" couples to the gluon field

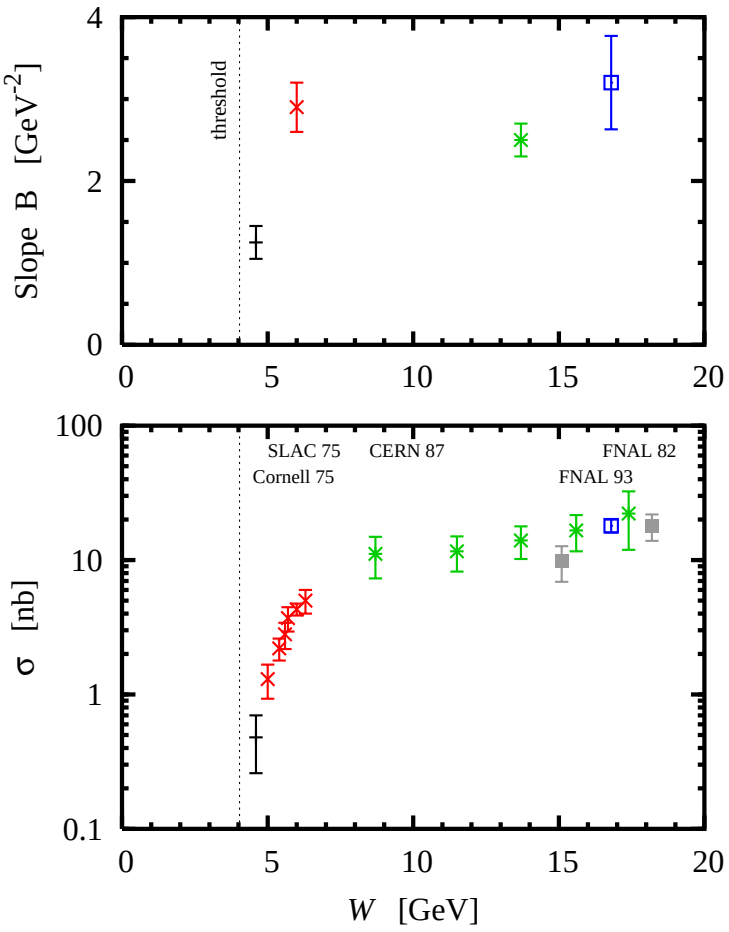

FIG. 25: B-slopes and total cross section data for J/ψ photoproduction shown over a wide range of photon-proton c.m. energies W. The proposed measurement will cover the region from threshold up to $W = 4.5$ GeV, below any existing data, with very good uncertainties (shown in Fig. 27).

in the target. Exclusive J/ψ production near threshold thus measures the nucleon form factor of a gluonic operator and can provide unique information on the non-perturbative gluon fields in the nucleon.

The precise identification of the gluonic operators associated with J/ψ production near threshold and the modeling of their nucleon form factors are the subject of intense theoretical research, the status and perspectives of which were summarized at a recent topical workshop [64]. Several approaches are presently being discussed. One scenario assumes that even near threshold the J/ψ is produced through two–gluon exchange with a GPD–like coupling to the nucleon, but now in the special kinematics of large $|t| \sim |t_{\rm min}|$ and large "skewness" $\xi \sim 0.5$ [65]. A more likely possibility is that the production process near threshold effectively reduces to a

local gluonic operator, implying simple kinematic scaling relations [66]. Another scenario uses the hard scattering mechanism for high-t elastic form factors and assumes that the production process happens in the leading 3-quark Fock component of the nucleon, with rescattering through hard gluon exchange [67]. J/psi production near threshold is also being studied in the non–relativistic QCD (NRQCD) scheme, which attempts a systematic parametric expansion in the heavy quark velocity [68, 69]; first results for JLab 12 GeV kinematics were reported in Ref. [70].

It is clear that progress with unraveling the mechanism of J/ψ production near threshold depends crucially on experimental input. Because of the small cross sections exclusive J/ψ production near threshold was never measured with the precision necessary to discriminate between the proposed dynamical scenarios, let alone to extract quantitative information on the relevant operators probing the color fields in the nucleon. The existing data from the SLAC and Cornell experiments [71, 72] (see Fig. 25) provide some rough information on the energy dependence of the exclusive photoproduction cross section and the t–slope near threshold. The present CLAS12 experiment represents a unique opportunity to explore the unmeasured near–threshold region from $E_\gamma \approx 8.5\,\mathrm{GeV}$ to $11\,\mathrm{GeV}$. The projected data would dramatically extend and improve our knowledge of the J/ψ photoproduction cross section and t–dependence near threshold (see Sect. 5 B), and directly impact on the on–going theoretical studies of the reaction mechanism.

Another fundamental question of QCD is the interaction of the J/ψ with nuclear matter, as described by the ψ–N scattering cross sections (elastic and inelastic) as functions of the relative energy. Several works in the literature attempt to relate the ψ–N interaction to the properties of non–perturbative color fields in QCD (see Ref. [58] and the presentations [64] for a recent review). In photo– and electroproduction experiments the ψ–N interaction can in principle be studied in two ways: (a) as final–state interaction in J/ψ production on the proton extremely close to threshold, ψ–N CM momenta $< 100\,\mathrm{MeV}$; (b) in J/ψ rescattering or absorption in production on nuclear targets. In both approaches reliable knowledge of the primary production amplitude on the proton is an essential prerequisite for extracting the ψ–N interaction. The measurement of the photoproduction cross section near threshold with CLAS12 would thus provide an excellent basis for future studies of the ψ–N interaction with 12 GeV.

The physics analysis of J/ψ production with CLAS12 and its impact on theoretical models will be described in a future proposal. That proposal will also address J/ψ electroproduction and nuclear targets, as outlined in our Letter of Intent (LOI11-106). Measurements on nuclear targets will be considered as a way to study the gluonic structure of nuclei and the $J/\psi - N$ interaction. The goals of the electroproduction measurements will be to map out the Q^2-dependence as an additional test of the hardness of the reaction (small size of the J/ψ), and constrain the ratio of the real and imaginary parts of the amplitude through measurements of interference structure functions. The electroproduction measurement will greatly benefit from the CLAS12 forward

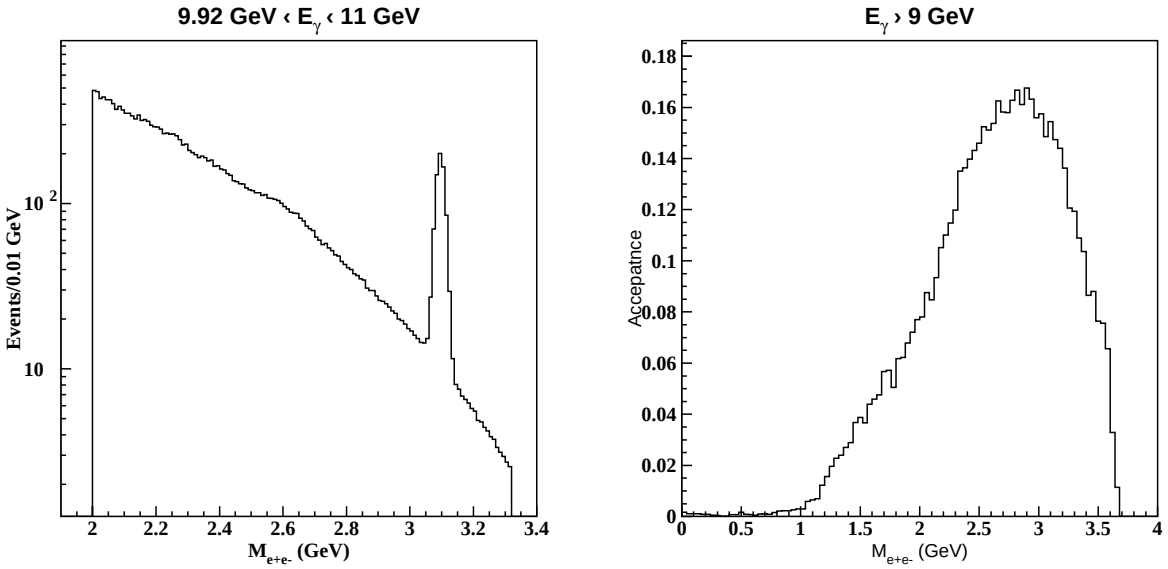

FIG. 26: *Left panel:* Exclusive J/ψ yield on a BH background as a function of the e^+e^- invariant mass for an incoming photon energy bin between 10 and 11 GeV. The J/ψ peak is clearly visible. *Right panel:* CLAS12 acceptance for the exclusive reaction $ep \to e^+e^-p(e')$ for photon energies between 9 and 11 GeV. In high-energy e^+e^- photoproduction, the CLAS12 acceptance for the $\phi(1020)$ is small.

tagger (FT), which will provide electron detection down to 2.5°, allowing a continuous coverage in Q^2 starting from a low value. Combined with the large acceptance of CLAS12, it gives for this reaction a good t–coverage and high rates.

B. Projected results

In this section we show the projected uncertainties for the total and differential, exclusive and inclusive J/ψ photoproduction cross sections. The same assumptions were made for the luminosity and running time as in Sect. 4. The acceptance simulations were also performed in a similar way. The mass spectrum for exclusive e^+e^- pair production and the corresponding acceptance are shown in Fig. 26.

To estimate the exclusive J/ψ photoproduction rate, we used the most conservative low-energy extrapolation of the SLAC/Cornell cross section data. Numerically, we used the parametrization labeled "2-gluon exchange" in Ref. [67], on which curve our projected data points are shown in the left panels of Figs. 27 and 28. For completeness, the parametrization labeled "3-gluon exchange" in Ref. [67] is also shown (upper curve), but was not used for

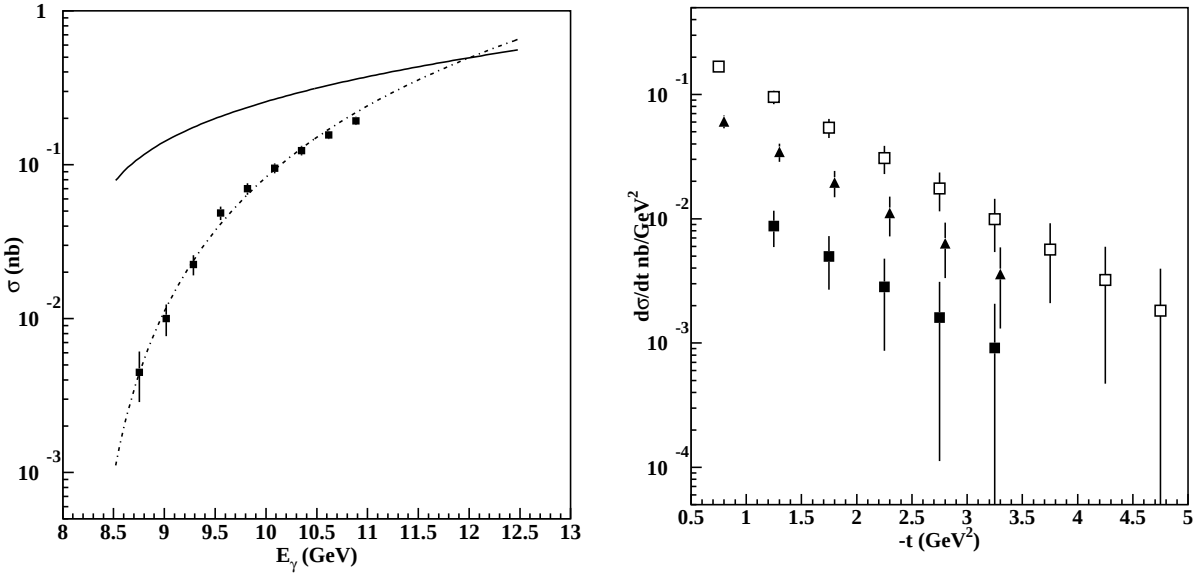

FIG. 27: Statistical uncertainties for exclusive J/ψ photoproduction in 100 days of running. *Left panel:* Total cross section as a function of incoming photon energy. The curves are calculated according to cross section formulas in Ref. [67]. *Right panel:* Differential cross section as a function of the four-momentum transfer $-t$ for three bins of s. The dashed line and the filled squares are for $s = 17.55$ to 18.05 GeV^2, the dotted line and the inverted filled triangles are for $s = 19.05$ to 19.55 GeV^2, and the dashed-dotted line and the open squares are for $s = 21.05$ to 21.55 GeV^2.

estimating rates or uncertainties.

The t-distribution for exclusive J/ψ photoproduction is shown in the right panel of Fig. 27 for three bins in s. The bottom curve (filled squares) shows a bin with an average incoming photon energy of 9 GeV, and the top curve (open squares) shows a bin centered at 10.8 GeV. The simulated data points show our statistical uncertainties for 100 days of running. Our projections for the total and differential cross sections for inclusive J/ψ photoproduction are shown in Fig. 28. Uncertainties are shown both for 100 days (filled squares) and 30 days (open squares), the latter corresponding to the requested beam time with reversed CLAS12 torus field. Should data support a flattening out of the cross section near threshold, the rates would be much higher and the projected uncertainties would shrink accordingly, giving exceptional precision even very close to threshold.

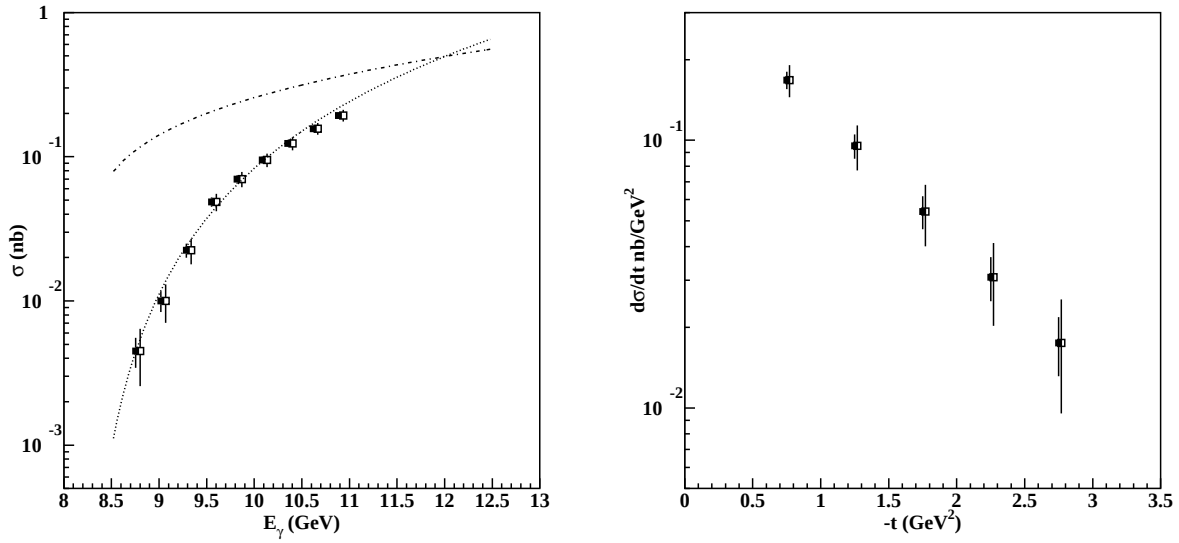

FIG. 28: Statistical uncertainties for inclusive J/ψ photoproduction, *i.e.*, $ep \to J/\psi X \to e^+e^-X$. The filled and open points correspond to 100 and 30 days of running, respectively. *Left panel:* Total cross section as a function of photon energy, with curves as in Fig. 27. *Right panel:* Differential cross section as a function of the four-momentum transfer for $s = 21.05$ to 21.55 GeV^2.

C. Impact on the TCS measurement

Due to its identical final state, the acceptance for exclusive J/ψ production is very similar to that of TCS events in the proposed range of lepton invariant mass. However, the narrow peak of the J/ψ, shown in the left panel of Fig. 26, is more suitable for a reliable yield extraction than the TCS-BH continuum. The J/ψ photoproduction reaction can thus serve as an important benchmark, allowing us to better understand the systematic uncertainties. The $\phi(1020)$ could in principle also be used in a similar way at the lower end of the invariant mass range, but as shown in the right panel of Fig. 26, the CLAS12 acceptance for ϕ photoproduction at high photon energy is small. A measurement of the J/ψ cross section in parallel with TCS will thus be very beneficial for the understanding the TCS data, and help addressing the two main sources of systematic uncertainty, *i.e.*, acceptance and lepton identification.

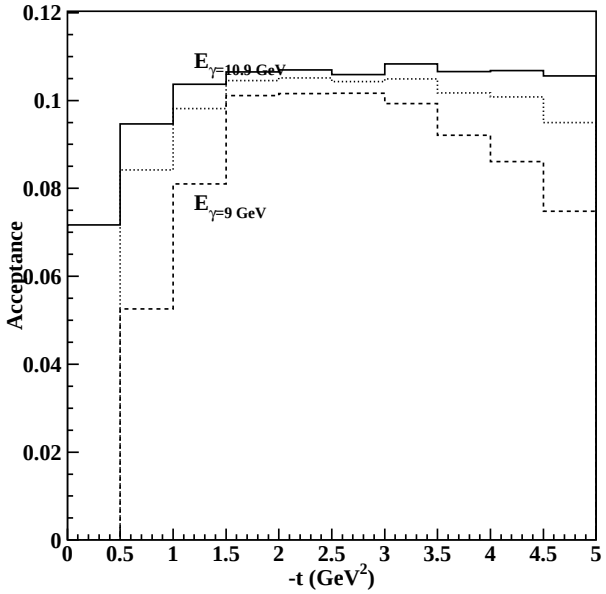

FIG. 29: CLAS12 acceptance for the reaction $ep \to J/\psi pX \to e^+e^-pX$ as a function of the four-momentum transfer for three bins in the incident photon energy ranging from 9 to 11 GeV.

6. SYSTEMATIC UNCERTAINTIES

The two main sources of systematic uncertainty for the proposed measurement are the acceptance corrections and lepton identification. The former can be expected to be similar to estimates for other cross section measurements with CLAS12, *i.e.*, to be at least of the order of 5%. As discussed in Sect. 4 A, the acceptance studies will be performed through simulations using GEMC – the standard GEANT4 package for CLAS12.

As described in Sect. 3 B, lepton identification will be performed using the high-threshold Cherenkov counter (HTCC) and the forward electromagnetic calorimeter (FEC). Fig. 20 further shows that all leptons used in the analysis will be detected in the FEC, and all but a few percent of the lepton pairs will have at least one lepton also detected in the HTCC. For those pairs, the two-pion rejection factor is expected to be at least 2×10^7. The remaining pairs can be discarded from the analysis without any significant impact on the statistical uncertainty.

In the photon-energy range of the proposed experiment, the total cross section for $\pi^+\pi^-$ production is 0.1 mb. With a pion pair rejection factor of 2×10^7, there would be a pion background at the 5% level if the total e^+e^- cross section was 0.1 nb. This is comparable to the J/ψ cross section alone in JLab 12 GeV kinematics. The BH cross section integrated over $0.5 < Q'^2 < 7$ GeV^2 at $E_\gamma = 11$ GeV is 34 nb. For most kinematics, and in particular those

in the primary range of interest (*i.e.*, for $4 < Q'^2 < 9$ GeV^2), the total uncertainty in the yield extraction would thus be dominated by statistics, with acceptance being the main source of systematic uncertainty.

A. Data with a reversed torus field

The uncertainties due to acceptance and lepton identification will depend on the actual performance of various elements of the CLAS12 detector, and imperfections in the event reconstruction or simulation. During the 6 GeV era, CLAS experiments like TPE have shown that taking e^+e^- data with both polarities of the CLAS torus field is invaluable for evaluating such uncertainties, and then possibly correcting for them. At least the former would be very important for a reliable interpretation of the TCS results, and in particular the extracted cosine moments. Thus, we propose to also take data with a reversed torus field. The data will include both exclusive and inclusive e^+e^- pair production. The evaluation of systematic uncertainties will also be greatly simplified by the fact that we can take TCS and J/ψ data in parallel.

For exclusive production, the acceptances with normal and reversed fields differ, as the outbending proton becomes inbending. A comparison will, however, allow us to cross check and optimize the acceptance simulations, and provide better estimates of the uncertainty due to acceptance. The extraction of the J/ψ cross section with both polarities of the torus fields will serve as a benchmark.

Due to the symmetry between electrons and positrons in normal and reversed torus fields, comparing inclusive e^+e^- production for the two settings would be ideal for pinning down the details the detector efficiency and understanding particle identification. Here, again, the J/ψ cross section will be a good benchmark. A simulation of the inclusive J/ψ acceptance for three incident photon energies ranging between 9 and 10.9 GeV is shown in Fig. 29. A combination of 100 days with regular and 30 days with reversed field will, as shown in Fig. 28, allow for a good comparison over a wide range in E_γ and $-t$. The statistical uncertainty for the inclusive J/ψ cross section with 30 days of running is also reasonably well matched with the expected systematic uncertainties in the acceptance.

7. BEAM TIME REQUEST

We request the equivalent of 100 PAC days with longitudinally polarized 11 GeV beam and an unpolarized proton target with the normal setting of the torus field, and an additional 30 days with a reversed field.

The first part of the beam-time request can be shared with already approved CLAS12 experiments. The proposed measurement imposes few demands on the running conditions, and can thus take full advantage of all the available beam time, It does, however, require the maximum beam energy. The already approved beam time that is suitable for this experiment covers 120 PAC days, of which at least 80 will be taken at full luminosity. We estimate this to be equivalent to 100 days at full luminosity. A polarization in excess of 80% has been assumed.

The second part of the beam-time request is for data to be taken with a reversed polarity of the CLAS torus field. In addition to providing more statistics, these data will be important for evaluating the systematic uncertainties associated with the CLAS12 acceptance for the outgoing e^+e^- pair, and for understanding the lepton identification.

These studies are important for the proposed TCS and J/ψ measurements, but will benefit all experiments during the run period. If the CLAS12 proton running is divided up into several blocks, the time with reversed field should preferably be scheduled in proportion to the amount of time in the standard configuration in each block.

[1] G. A. Miller, M. Strikman, and C. Weiss. Pion transverse charge density from timelike form factor data. *Phys. Rev. D*, 83:013006, Jan 2011, arXiv:1011.1472 [hep-ph].

[2] K. Goeke, M.V. Polyakov, and M. Vanderhaeghen. Hard exclusive reactions and the structure of hadrons. *Progress in Particle and Nuclear Physics*, 47(2):401 – 515, 2001, hep-ph/0106012.

[3] M. Diehl. Generalized parton distributions. *Physics Reports*, 388(24):41 – 277, 2003, hep-ph/0307382.

[4] A.V. Belitsky and A.V. Radyushkin. Unraveling hadron structure with generalized parton distributions. *Physics Reports*, 418(16):1 – 387, 2005, hep-ph/0504030.

[5] John C. Collins, Leonid Frankfurt, and Mark Strikman. Factorization for hard exclusive electroproduction of mesons in qcd. *Phys. Rev. D*, 56:2982–3006, Sep 1997, hep-ph/9611433.

[6] John C. Collins and Andreas Freund. Proof of factorization for deeply virtual compton scattering in qcd. *Phys. Rev. D*, 59:074009, Feb 1999, hep-ph/9801262.

[7] Xiangdong Ji. Gauge-invariant decomposition of nucleon spin. *Phys. Rev. Lett.*, 78:610–613, Jan 1997, hep-ph/9603249.

[8] E.R. Berger, M. Diehl, and B. Pire. Timelike compton scattering: exclusive photoproduction of lepton pairs. *The European Physical Journal C - Particles and Fields*, 23:675–689, 2002, hep-ph/0110062.

[9] M. Guidal. A Fitter code for Deep Virtual Compton Scattering and Generalized Parton Distributions. *Eur. Phys. J.*, A37:319–332, 2008, arXiv:0807.2355 [hep-ph].

[10] B. Pire, L. Szymanowski, and J. Wagner. Can one measure timelike compton scattering at lhc?. *Phys. Rev. D*, 79:014010, Jan 2009, arXiv:0811.0321 [hep-ph].

[11] B. Pire, L. Szymanowski, and J. Wagner. Next-to-leading order corrections to timelike, spacelike, and double deeply virtual compton scattering. *Phys. Rev. D*, 83:034009, Feb 2011, arXiv:1101.0555 [hep-ph].

[12] D. Müller, B. Pire, L. Szymanowski, and J. Wagner. On timelike and spacelike hard exclusive reactions. 2012, arXiv:1203.4392 [hep-ph].

[13] M.V. Polyakov and A.G. Shuvaev. On'dual' parametrizations of generalized parton distributions. 2002, hep-ph/0207153.

[14] V. Guzey and T. Teckentrup. The Dual parameterization of the proton generalized parton distribution functions H and E and description of the DVCS cross sections and asymmetries. *Phys. Rev.*, D74:054027, 2006, hep-ph/0607099.

[15] V. Guzey and T. Teckentrup. On the mistake in the implementation of the minimal model of the dual parameterization and resulting inability to describe the high-energy DVCS data. *Phys. Rev.*, D79:017501, 2009, arXiv:0810.3899 [hep-ph].

[16] Maxim V. Polyakov and Kirill M. Semenov-Tian-Shansky. Dual parametrization of GPDs versus double distribution Ansatz. *Eur. Phys. J.*, A40:181–198, 2009, arXiv:0811.2901 [hep-ph].

[17] A.V. Radyushkin. Double distributions and evolution equations. *Phys. Rev.*, D59:014030, 1999, hep-ph/9805342.

[18] M. V. Polyakov and C. Weiss. Skewed and double distributions in the pion and the nucleon. *Phys. Rev. D*, 60:114017, Nov 1999, hep-ph/9902451.

[19] R. L. Jaffe and Aneesh Manohar. The G(1) Problem: Fact and Fantasy on the Spin of the Proton. *Nucl. Phys.*, B337:509–546, 1990, [INSPIRE].

[20] M. V. Polyakov. Generalized parton distributions and strong forces inside nucleons and nuclei. *Phys. Lett.*, B555:57–62, 2003, hep-ph/0210165.

[21] K. Goeke et al. Nucleon form-factors of the energy momentum tensor in the chiral quark-soliton model. *Phys. Rev.*, D75:094021, 2007, hep-ph/0702030.

[22] M. Gockeler et al. Generalized parton distributions from lattice QCD. *Phys. Rev. Lett.*, 92:042002, 2004, hep-ph/0304249.

[23] I.V. Anikin and O.V. Teryaev. Dispersion relations and subtractions in hard exclusive processes. *Phys. Rev.*, D76:056007, 2007, arXiv:0704.2185 [hep-ph].

[24] M. Diehl and D. Yu. Ivanov. Dispersion representations for hard exclusive processes: beyond the Born approximation. *Eur. Phys. J.*, C52:919–932, 2007, arXiv:0707.0351 [hep-ph].

[25] M.V. Polyakov. Tomography for amplitudes of hard exclusive processes. *Phys. Lett.*, B659:542–550, 2008, arXiv:0707.2509 [hep-ph].

[26] Stanley J. Brodsky, Francis E. Close, and J.F. Gunion. Compton scattering and fixed poles in parton field theoretic models. *Phys. Rev.*, D5:1384, 1972, [INSPIRE].

[27] Stanley J. Brodsky, Francis E. Close, and J.F. Gunion. Phenomenology of Photon Processes, Vector Dominance and Crucial Tests for Parton Models. *Phys. Rev.*, D6:177, 1972, [INSPIRE].

[28] Stanley J. Brodsky, Francis E. Close, and J.F. Gunion. A gauge - invariant scaling model of current interactions with regge behavior and finite fixed pole sum rules. *Phys. Rev.*, D8:3678, 1973, [INSPIRE].

[29] Stanley J. Brodsky, Felipe J. Llanes-Estrada, and Adam P. Szczepaniak. Local Two-Photon Couplings and the J=0 Fixed Pole in Real and Virtual Compton Scattering. *Phys. Rev.*, D79:033012, 2009, arXiv:0812.0395 [hep-ph].

[30] V. Yu. Petrov et al. Off-forward quark distributions of the nucleon in the large N(c) limit. *Phys. Rev.*, D57:4325–4333, 1998, hep-ph/9710270.

[31] Andreas Freund and Martin McDermott. Next-to-leading order qcd analysis of deeply virtual compton scattering amplitudes. *Phys. Rev. D*, 65:074008, Mar 2002, hep-ph/0106319.

[32] A. Freund and M. McDermott. A next-to-leading order analysis of deeply virtual compton scattering. *Phys. Rev. D*, 65:091901, Apr 2002, hep-ph/0106124.

[33] A. Freund and M. McDermott. A detailed next-to-leading order qcd analysis of deeply virtual compton scattering observables. *The European Physical Journal C - Particles and Fields*, 23:651–674, 2002, hep-ph/0111472.

[34] H. Moutarde, B. Pire, F. Sabatie, L. Szymanowski, and J. Wagner. work in preparation.

[35] I. V. Anikin, B. Pire, L. Szymanowski, O. V. Teryaev, and S. Wallon. On BLM scale fixing in exclusive processes. *The European Physical Journal C - Particles and Fields*, 42:163–168, 2005, hep-ph/0411408.

[36] Xiangdong Ji and Jonathan Osborne. One-loop corrections and all order factorization in deeply virtual compton scattering. *Phys. Rev. D*, 58:094018, Sep 1998, hep-ph/9801260.

[37] Xiangdong Ji and Jonathan Osborne. One-loop qcd corrections to deeply-virtual compton scattering: The parton helicity-independent case. *Phys. Rev. D*, 57:1337–1340, Feb 1998, hep-ph/9707254.

[38] L. Mankiewicz, G. Piller, E. Stein, M. Vänttinen, and T. Weigl. NLO corrections to deeply-virtual

Compton scattering. *Physics Letters B*, 425(12):186 – 192, 1998, hep-ph/9712251.

[39] A.V. Belitsky and D. Müller. Predictions from conformal algebra for the deeply virtual compton scattering. *Physics Letters B*, 417(12):129 – 140, 1998, hep-ph/9709379.

[40] A.V. Belitsky, D. Müller, L. Niedermeier, and A. Schäfer. Deeply virtual compton scattering in next-to-leading order. *Physics Letters B*, 474(12):163 – 169, 2000, hep-ph/9908337.

[41] K. Kumericki, D. Müller, and K. Passek-Kumericki. Towards a fitting procedure for deeply virtual compton scattering at next-to-leading order and beyond. *Nuclear Physics B*, 794(12):244 – 323, 2008, hep-ph/0703179 [HEP-PH].

[42] H. Moutarde. Extraction of the compton form factor $\mathcal{H}$ from deeply virtual compton scattering measurements at jefferson lab. *Phys. Rev. D*, 79:094021, May 2009, arXiv:0904.1648 [hep-ph].

[43] M. Guidal and H. Moutarde. Generalized parton distributions from deeply virtual compton scattering at hermes. *The European Physical Journal A - Hadrons and Nuclei*, 42:71–78, 2009, arXiv:0905.1220 [hep-ph].

[44] M. Guidal. Generalized parton distributions from deep virtual compton scattering at CLAS. *Physics Letters B*, 689(45):156 – 162, 2010, arXiv:1003.0307 [hep-ph].

[45] M. Guidal. Constraints on the generalized parton distribution from deep virtual compton scattering measured at hermes. *Physics Letters B*, 693(1):17 – 23, 2010, arXiv:1005.4922 [hep-ph].

[46] H. Moutarde and [on behalf of the CLAS group]. Extraction of the Compton form factor H from DVCS measurements in the quark sector. In *AIP Conference Proceedings*, volume 1374, pages 133–138. American Insitute of Physics, 2011, arXiv:1010.4521 [hep-ph].

[47] H. Moutarde and [on behalf of the CLAS group at Saclay]. Extraction of the compton form factor H from recent DVCS measurements at jlab. In *Exclusive Reactions at High Momentum Transfer: Proceedings of the 4th Workshop*, pages 53–60. World Scientific, 2011, INSPIRE.

[48] K. Kumericki, D. Mueller, and A. Schafer. Parametrizing compton form factors with neural networks. 2011, arXiv:1112.1958 [hep-ph]. Presented by K.K. at Ringberg HERA workshop.

[49] M. Vanderhaeghen, Pierre A.M. Guichon, and M. Guidal. Deeply virtual electroproduction of photons and mesons on the nucleon: Leading order amplitudes and power corrections. *Phys. Rev.*, D60:094017, 1999, hep-ph/9905372.

[50] M. Guidal, M.V. Polyakov, A.V. Radyushkin, and M. Vanderhaeghen. Nucleon form-factors from generalized parton distributions. *Phys. Rev.*, D72:054013, 2005, hep-ph/0410251.

[51] R. Paremuzyan. *Timelike Compton Scattering*. PhD thesis, Yerevan, 2010.

[52] B.A. Mecking et al. The cebaf large acceptance spectrometer (clas). *Nucl. Instrum. Meth.*, A503:513–553, 2003.

[53] CLAS12 technical design report. Technical report, JLAB, 2008.

[54] Event generator for electro- and photoproduction on nucleon and nuclei, 2005. CLAS software repository.

[55] Bethe-heitler code. CLAS software repository.

[56] Monte-carlo program to simulate CLAS12 detector response. CLAS software repository.

[57] V. Guzey. Code for cross section calculations for Bethe-Heitler and Timelike Compton Scattering.

[58] N. Brambilla, S. Eidelman, B.K. Heltsley, R. Vogt, G.T. Bodwin, et al. Heavy quarkonium: progress, puzzles, and opportunities. *Eur. Phys. J.*, C71:1534, 2011, arXiv:1010.5827 [hep-ph].

[59] Leonid Frankfurt, Mark Strikman, and Christian Weiss. Small-x physics: From HERA to LHC and

beyond. *Ann. Rev. Nucl. Part. Sci.*, 55:403–465, 2005, hep-ph/0507286.

[60] A. Aktas et al. Elastic J/psi production at HERA. *Eur. Phys. J.*, C46:585–603, 2006, hep-ex/0510016.

[61] S. Chekanov et al. Exclusive electroproduction of J/psi mesons at HERA. *Nucl. Phys.*, B695:3–37, 2004, hep-ex/0404008.

[62] Morris E. Binkley, C. Bohler, J. Butler, John P. Cumalat, I. Gaines, et al. J/psi Photoproduction from 60-GeV/c to 300-GeV/c. *Phys. Rev. Lett.*, 48:73, 1982, [INSPIRE].

[63] Daniel Boer, Markus Diehl, Richard Milner, Raju Venugopalan, Werner Vogelsang, et al. Gluons and the quark sea at high energies: Distributions, polarization, tomography. 2011, arXiv:1108.1713 [nucl-th].

[64] Workshop on non-perturbative color forces in qcd, March 2012, http://quarks.temple.edu/∼npcfiqcd/.

[65] Leonid Frankfurt and Mark Strikman. Two gluon form-factor of the nucleon and J / psi photoproduction. *Phys. Rev.*, D66:031502, 2002, hep-ph/0205223.

[66] C. Weiss and M. Strikman. Probing color fields with heavy quarkonia [in progress]. In *Workshop on Non-Perturbative Color Forces in QCD*. Temple University, Philadelphia, PA, 2012, http://quarks.temple.edu/∼npcfiqcd/.

[67] S.J. Brodsky, E. Chudakov, P. Hoyer, and J.M. Laget. Photoproduction of charm near threshold. *Phys. Lett.*, B498:23–28, 2001, hep-ph/0010343.

[68] Mathias Butenschoen and Bernd A. Kniehl. Complete next-to-leading-order corrections to J/psi photoproduction in nonrelativistic quantum chromodynamics. *Phys. Rev. Lett.*, 104:072001, 2010, arXiv:0909.2798 [hep-ph].

[69] Mathias Butenschoen and Bernd A. Kniehl. World data of J/psi production consolidate NRQCD factorization at NLO. *Phys. Rev.*, D84:051501, 2011, arXiv:1105.0820 [hep-ph].

[70] Mathias Butenschoen and Bernd A. Kniehl. Non-relativistic qcd in heavy quarkonium production. In *Workshop on Non-Perturbative Color Forces in QCD*. Temple University, Philadelphia, PA, 2012, http://quarks.temple.edu/∼npcfiqcd/.

[71] B. Gittelman, K. M. Hanson, D. Larson, E. Loh, A. Silverman, and G. Theodosiou. Photoproduction of the $\psi(3100)$ meson at 11 gev. *Phys. Rev. Lett.*, 35:1616–1619, Dec 1975, INSPIRE.

[72] U. Camerini, J. G. Learned, R. Prepost, C. M. Spencer, D. E. Wiser, W. W. Ash, R. L. Anderson, D. M. Ritson, D. J. Sherden, and C. K. Sinclair. Photoproduction of the ψ particles. *Phys. Rev. Lett.*, 35:483–486, Aug 1975, INSPIRE.